Article

Discovery Medicine 2025; 37(202): 2765–2785
https://doi.org/10.24976/Discov.Med.202537202.231

PTPRO Deficiency Alleviates Ulcerative Colitis by Increasing the Treg/Th1 Ratio Through JAK2-STAT5 Pathway Activation

Xianlan Zhu[1,†], Xujin Chen[1,†], Ruyi Huang[2], Lin Ji[1], Jiale Lv[1], Wenying Tian[1], Cheng Yang[1], Mingming Wang[3,*], Lijuan Xu[4,*]

[1]Department of Gastroenterology, The Affiliated Wuxi People's Hospital of Nanjing Medical University, Wuxi People's Hospital, Wuxi Medical Center, Nanjing Medical University, 214023 Wuxi, Jiangsu, China
[2]Department of General Surgery, The Affiliated Wuxi People's Hospital of Nanjing Medical University, Wuxi People's Hospital, Wuxi Medical Center, Nanjing Medical University, 214023 Wuxi, Jiangsu, China
[3]Department of General Surgery, The Affiliated Jiangning Hospital of Nanjing Medical University, 210000 Nanjing, Jiangsu, China
[4]Department of Gastroenterology, The Affiliated Suzhou Hospital of Nanjing Medical University, Suzhou Municipal Hospital, Gusu School, Nanjing Medical University, 215008 Suzhou, Jiangsu, China
*Correspondence: ljxualexis@126.com (Lijuan Xu); jswmm2001@163.com (Mingming Wang)
[†]These authors contributed equally.
Submitted: 21 July 2025 Revised: 1 October 2025 Accepted: 22 October 2025 Published: 20 November 2025

Background: Ulcerative colitis (UC) is a chronic inflammatory bowel disease (IBD) characterized by immune dysregulation, particularly the imbalance between T helper 1 (Th1) and regulatory T (Treg) cells, which plays a crucial role in its pathogenesis. Members of the protein tyrosine phosphatase (PTP) family are involved in immune regulation, and the protein tyrosine phosphatase receptor-type O (PTPRO) is significantly upregulated in inflamed tissues. However, the specific role of PTPRO in UC remains unclear. This study aimed to investigate the role and mechanisms of PTPRO in UC to identify new therapeutic targets.
Methods: A mouse model of UC was induced using dextran sulfate sodium (DSS), and PTPRO expression was examined in the colonic tissues of both mice and UC patients. PTPRO knockout ($PTPRO^{-/-}$) mice were used to assess the impact of PTPRO deficiency on UC severity and the regulation of Th1/Treg cell balance. Primary T cells were isolated from mice to explore the signaling pathways regulated by PTPRO.
Results: PTPRO expression was significantly elevated in inflamed colonic tissues from both DSS-treated mice and UC patients ($p < 0.05$). $PTPRO^{-/-}$ mice exhibited attenuated colitis, manifesting as reduced body weight loss, lower Disease Activity Index (DAI) scores, and markedly improved histopathology compared to wild-type (WT) mice (all $p < 0.05$). Knockout of PTPRO reduced colonic levels of pro-inflammatory cytokines (interferon-γ (IFN-γ), tumor necrosis factor-α (TNF-α), interleukin-6 (IL-6), and interleukin-1β (IL-1β)) while increasing anti-inflammatory mediators (interleukin-10 (IL-10) and Forkhead box P3 (Foxp3)) ($p < 0.05$). Consistently, flow cytometry analysis demonstrated that $PTPRO^{-/-}$ mice had fewer Th1 cells and more Tregs in the colon, suggesting the restoration of immune homeostasis ($p < 0.05$). Mechanistically, PTPRO was found to interact with Janus kinase 2 (JAK2) and function as a negative regulator of JAK2–signal transducer and activator of transcription 5 (STAT5) signaling. Loss of PTPRO led to increased phosphorylation of JAK2 and STAT5, thereby promoting Treg differentiation, whereas *in vivo* JAK2 inhibition reversed these effects.
Conclusion: PTPRO regulates the Th1/Treg balance via the JAK2-STAT5 pathway, and its absence shifts the immune response toward anti-inflammatory Tregs, highlighting PTPRO as a potential therapeutic target for UC.

Keywords: PTPRO; ulcerative colitis; Th1/Treg balance; T-cell immunity; JAK2-STAT5 pathway

Introduction

Ulcerative colitis (UC) is a chronic, relapsing form of inflammatory bowel disease (IBD) characterized by abnormal immune responses in the colonic mucosa [1,2]. A hallmark of UC is an imbalanced ratio of pro-inflammatory T helper 1 (Th1) cells to immunosuppressive regulatory T (Treg) cells [3,4]. Excessive Th1 activation, coupled with overproduction of cytokines such as interferon-γ (IFN-γ) and tumor necrosis factor-α (TNF-α), drives sustained intestinal inflammation, while insufficient Treg activity fails to adequately counteract this damage [5]. Restoring the Th1/Treg balance has emerged as a promising therapeutic strategy for UC [6,7]. Recent research has demonstrated that shifting immune responses away from pathogenic Th1/Th17 cells and toward Tregs can alleviate experimental colitis [8].

Protein tyrosine phosphatases (PTPs) have emerged as important modulators of immune cell signaling and fate [9]. By counterbalancing the actions of protein tyrosine kinases, PTPs precisely regulate signaling pathways governing immune cell activation, differentiation, and tolerance [10,11]. Dysregulation of PTP activity is implicated in various diseases, including autoimmunity and chronic inflammation [12]. Protein tyrosine phosphatase receptor-type O (PTPRO), a member of the R3 subtype of receptor-like PTPs, has been linked to immune regulatory processes [13]. Notably, PTPRO exists in two major forms: a full-length variant predominantly expressed in certain epithelial tissues and a truncated isoform, PTPROt, present in hematopoietic cells such as B cells, T cells, and macrophages [14]. This tissue-specific expression pattern suggests that PTPRO may fulfill distinct functions in immune cells. Accumulating evidence indicates that PTPRO promotes inflammatory responses in multiple disease contexts [15]. For example, following spinal cord injury, activated microglia upregulate PTPRO, and knockdown of PTPRO in microglia polarizes them toward an anti-inflammatory M2 phenotype while reducing pro-inflammatory M1 markers. In lung inflammation models, PTPRO similarly exacerbates inflammatory responses: silencing PTPRO in human pulmonary cells attenuates lipopolysaccharide (LPS)-induced cytokine release and apoptosis, whereas PTPRO overexpression worsens injury by potentiating toll-like receptor 4 (TLR4)/nuclear factor-κB (NF-κB) signaling [16]. Consistent with these findings, PTPRO expression is elevated in other inflammation-associated conditions [17]. Deletion or inhibition of PTPRO in obese mice, for instance, prevents ectopic fat accumulation and produces a “healthy obesity” phenotype characterized by dramatically reduced systemic inflammation [18]. Similarly, the immune-specific isoform PTPRO has been shown to aggravate chronic inflammatory liver disease by driving NF-κB activation in liver macrophages, thereby exacerbating nonalcoholic steatohepatitis (NASH) [19]. Conversely, in certain cancer settings, PTPROt may support anti-tumor immunity; for example, PTPROt helps maintain T cell surveillance in hepatocellular carcinoma [20]. Collectively, these studies demonstrate that PTPRO can modulate immune cell polarization and function in a context-dependent manner, predominantly favoring pro-inflammatory roles in pathological inflammation.

Despite increasing recognition of PTPRO’s involvement in immune regulation, its specific role in IBD remains largely unexplored. Although PTPRO expression is elevated in colonic tissues of UC patients and may exacerbate intestinal inflammation via the TLR4/NF-κB pathway [21], the impact of PTPRO on adaptive immune cell dynamics in UC, particularly the critical Th1/Treg balance, remains poorly understood. Given the importance of proper T cell regulation for intestinal homeostasis, we hypothesized that PTPRO might influence UC severity by modulating T cell responses. Furthermore, PTPRO has been predicted to interact with key cytokine signaling molecules [22]. Previous research has demonstrated that PTPRO can bind to and dephosphorylate Janus kinase 2 (JAK2), a tyrosine kinase upstream of signal transducer and activator of transcription 5 (STAT5) that is essential for Forkhead box P3 (Foxp3)$^+$ Treg development (mediated by interleukin-2 (IL-2) signaling) [23]. This led us to postulate that PTPRO might regulate Treg differentiation through the JAK2-STAT5 pathway.

In this study, we examined PTPRO expression and function in UC using both human and mouse models. First, we measured PTPRO expression in colonic biopsy specimens from UC patients and in dextran sulfate sodium (DSS)-induced colitic mice to establish clinical and experimental relevance. We then employed PTPRO knockout (PTPRO$^{-/-}$) mice to assess how the absence of this phosphatase affects colitis severity, immune cell infiltration, and the Th1/Treg balance in the gut. We also performed *in vitro* CD4$^+$ T cell polarization assays to determine whether PTPRO intrinsically directs T cells toward the Th1 or Treg lineage. Finally, we investigated the involvement of the JAK2-STAT5 axis by examining PTPRO-JAK2 interactions and by pharmacologically manipulating this pathway. Our findings reveal a novel mechanism whereby PTPRO deficiency shifts the immune response toward anti-inflammatory Tregs via enhanced STAT5 phosphorylation, resulting in ameliorated colitis. These results provide mechanistic insight into PTPRO’s role in intestinal inflammation and identify PTPRO as a potential therapeutic target for restoring immune tolerance in UC.

Materials and Methods

Animals

For all experiments, we used wild-type (WT) C57BL/6J male mice and PTPRO knockout (PTPRO$^{-/-}$) mice, aged 6–8 weeks (weighing approximately 20 g). PTPRO$^{-/-}$ mice were originally generated on a C57BL/6J background and obtained from the Shanghai Laboratory Animal Center (Shanghai, China; License No. SYXK (Shanghai) 2021-0012). The knockout genotype was confirmed by polymerase chain reaction (PCR) analysis. All animals were housed under specific pathogen-free (SPF) conditions (22 $\pm$ 2 °C, 50–60% humidity, 12 h light/dark cycle) and provided standard chow and water *ad libitum*. Mice were acclimated to the facility for at least one week before experimentation. All procedures were approved by the Institutional Animal Ethics Committee (Approval No. IEC2023051201) and were performed in accordance with institutional and national guidelines for the care and use of laboratory animals.

A total of 88 mice were used in this study. Mice were assigned to the following groups: NC + WT group, NC + PTPRO$^{-/-}$ group, DSS + WT group, and DSS + PTPRO$^{-/-}$ group, with 10 mice per group. For the

AZD1480 treatment experiment, mice were assigned to DSS + WT group, DSS + PTPRO$^{-/-}$ group, and DSS + PTPRO$^{-/-}$ + AZD1480 group, with 10 mice per group. For flow cytometry analysis, mice were assigned to NC + WT group, DSS + WT group, and DSS + PTPRO$^{-/-}$ group, with 6 mice per group.

DSS-Induced Colitis

Acute colitis was induced by administering DSS in the drinking water, following established protocols. In brief, age- and sex-matched WT and PTPRO$^{-/-}$ mice received 5% (w/v) DSS (36–50 kDa; 0216011010, MP Biomedicals, CA, USA) in their drinking water for five consecutive days (day 0 through day 5) to induce mucosal injury. After day 5, DSS was removed and replaced with normal drinking water for an additional 7 days (until day 12) to allow colitis to fully develop. Control mice (normal controls) received plain water without DSS for the entire period. Each experimental group consisted of 8–10 mice, and each experiment was performed at least twice to ensure reproducibility [24].

To examine the role of JAK2-STAT5 signaling, a subset of mice was treated with the JAK2 inhibitor AZD1480 (HY-10193, MedChemExpress, Monmouth Junction, NJ, USA) concurrently with DSS exposure. Mice received drinking water containing 5% DSS *ad libitum* beginning on the morning of day 0, and the first dose of AZD1480 was administered via intraperitoneal injection between 15:00 and 16:00 on the same day. AZD1480 was dissolved in 10% dimethyl sulfoxide (DMSO) in phosphate-buffered saline (PBS) and administered via intraperitoneal (i.p.) injection at 30 mg/kg once daily, starting on day 0 (the first day of DSS exposure) and continuing throughout the DSS treatment period. Control animals for this intervention received i.p. injections of an equal volume of vehicle (10% DMSO/PBS) on the same schedule. All mice were monitored daily for clinical signs of colitis (weight loss, stool consistency, and fecal blood). At defined endpoints (day 5 to assess acute injury, and day 12 for peak disease), mice were humanely euthanized by CO_2 asphyxiation followed by cervical dislocation.

Clinical Symptom Assessment

Colitis severity was monitored using a Disease Activity Index (DAI) that combines scores for weight loss, stool consistency, and fecal bleeding. Mice were assessed daily for each parameter, as follows:

- Weight loss: 0 = no loss (or $<$1%); 1 = 1–6% loss; 2 = 6–12% loss; 3 = 12–18% loss; 4 = $>$18% loss of initial body weight.
- Stool consistency: 0 = normal well-formed pellets; 1 = soft but still formed; 2 = soft and semi-formed; 3 = very soft, almost liquid; 4 = watery diarrhea.
- Fecal bleeding: 0 = none (hemoccult-negative); 1 = trace occult blood; 2 = positive occult blood (red-tinged stool); 3 = grossly visible blood in stool; 4 = severe rectal bleeding.

Each mouse's DAI was calculated by summing the three subscores (maximum total = 12), with higher values indicating more severe colitis. All scoring was performed by observers blinded to the mice's genotype and treatment group [25].

Tissue Collection and Processing

Mice were euthanized on day 5 (acute injury) and days 10–12 (established inflammation and healing). The entire colon was removed and its length measured from the ileocecal junction to the anus as an indicator of inflammation. A 1-cm segment of distal colon was fixed in 10% neutral-buffered formalin for histology. The remaining tissue was opened longitudinally, rinsed with cold PBS, and divided for protein or RNA analysis. Protein samples were snap-frozen in liquid nitrogen and stored at –80 °C. RNA samples were placed in RNAlater solution (AM7023M, Thermo Fisher Scientific, Waltham, MA, USA) or immediately homogenized in TRIzol reagent.

In experiments involving AZD1480, tissue collection was performed at the end of the experiment (day 12) for all groups. Colonic samples from all mice (treatment and control) were processed in parallel to ensure consistent handling.

For the human studies, colonic biopsy specimens were obtained from UC patients and non-IBD controls during endoscopy and either snap-frozen in liquid nitrogen for molecular analyses or fixed in formalin for histology. This study was approved by the Ethics Committee of the Affiliated Wuxi People's Hospital of Nanjing Medical University (Approval No. KY23087) and conducted in accordance with the Declaration of Helsinki. Written informed consent was obtained from all patients for the human samples included in the study.

Real-Time Quantitative PCR (RT-qPCR)

Total RNA was extracted from mouse colonic tissue (and from human colonic biopsies) using TRIzol reagent (15596026CN, Invitrogen, Carlsbad, CA, USA) following the manufacturer's instructions. RNA purity and concentration were assessed by spectrophotometry, with A260/A280 ratios of approximately 2.0 indicating high purity. For each sample, 1 µg of total RNA was reverse-transcribed into complementary DNA (cDNA) using a high-capacity cDNA synthesis kit (170-8843, Bio-RAD, Hercules, CA, USA) with random hexamer primers. The resulting cDNA was used as the template for quantitative PCR, which was performed on a QuantStudio 6 Flex system (Applied Biosystems, Thermo Fisher Scientific, Waltham, MA, USA). We used SYBR Green PCR Master Mix (1725850, Bio-RAD, Hercules, CA, USA) and gene-specific primers to amplify targets of interest. Primer sequences for mouse target genes (e.g., *IFN-*γ, *TNF-*α, interleukin-6 (*IL-6*), and interleukin-1β (*IL-1*β), interleukin-10 (*IL-10*), *Foxp3*, etc.) and human *PTPRO* (plus reference genes) were designed based on pub-

lished sequences and are provided in **Supplementary Table 1**. Each qPCR reaction (10–20 µL volume) contained cDNA (equivalent to ~50 ng of input RNA), forward and reverse primers (300 nM each), and 1× SYBR Green master mix. The thermal cycling program was: 95 °C for 2 min; then 40 cycles of 95 °C for 15 s and 60 °C for 30 s. A melting curve analysis was performed at the end to confirm that a single specific PCR product was amplified. All samples were run in triplicate, and no-template control wells were included to monitor for contamination. The housekeeping gene glyceraldehyde 3-phosphate dehydrogenase (*GAPDH*) (for mouse samples) or *GAPDH* (for human samples) was used as an internal reference to normalize gene expression. Relative mRNA expression levels were calculated by the $2^{-\Delta\Delta Ct}$ method, normalizing each sample to the appropriate control group (e.g., untreated healthy mice or healthy human controls). Results are expressed as fold-change relative to controls (mean ± SD).

Histological Analysis

For histopathology, formalin-fixed colon segments were processed, embedded in paraffin, and cut into 4-µm-thick sections mounted on glass slides. Hematoxylin and eosin (H&E) staining was performed on deparaffinized sections using standard protocols to evaluate overall tissue morphology and inflammation. An experienced pathologist, blinded to sample identity, scored the H&E-stained sections for histopathological damage based on the following criteria: inflammatory cell infiltration (graded 0 = none; 1 = mild; 2 = moderate; 3 = severe), depth of injury (0 = none; 1 = mucosal; 2 = mucosal + submucosal; 3 = transmural), presence of ulceration (0 = none; 1 = small focal ulcers; 2 = moderate ulcers; 3 = large extensive ulcers), and crypt architectural distortion (0 = normal; 1 = mild goblet cell loss and gland disarray; 2 = significant goblet cell depletion and gland drop-out; 3 = crypt abscesses or complete gland loss). The individual component scores were summed to yield an overall histology score per sample (maximum score of 12).

Adjacent sections were stained with Alcian Blue/Periodic Acid-Schiff (AB/PAS; G1285, Solarbio, Beijing, China) to visualize goblet cells and mucins. In this combined stain, AB labels acidic mucins in goblet cell vacuoles (blue), while the PAS reagent counterstains other tissue elements (magenta). Goblet cell abundance was quantified by counting AB–positive goblet cells per colonic crypt in well-oriented regions, with at least 10–20 crypts counted per mouse. Micrographs were acquired using a light microscope (BX43, Olympus, Tokyo, Japan) equipped with a digital camera. Representative images at 100× and 200× magnification are presented in the figures.

Enzyme-Linked Immunosorbent Assay (ELISA)

Tissue levels of key cytokines were measured using enzyme-linked immunosorbent assays (ELISAs). Approximately 50 mg of colon tissue per sample was homogenized in lysis buffer (PBS with 0.1% Tween-20 plus protease/phosphatase inhibitor cocktail) using a bead mill or mechanical homogenizer. The homogenates were then centrifuged at 12,000 ×g for 15 min at 4 °C, and the clarified supernatants were collected. Total protein concentration in each sample was determined with a bicinchoninic acid (BCA) protein assay kit (23227, Pierce, Thermo Fisher Scientific, Waltham, MA, USA). Commercial ELISA kits for mouse IFN-γ, TNF-α, IL-6, IL-1β, and IL-10 (EMC101g.96, EMC102a.96, EMC004.96, EMC001b.96, and EMC005.96, Neobioscience, Guangdong, China) were used according to the manufacturers' protocols. Briefly, 96-well plates pre-coated with capture antibodies were loaded with standards and appropriately diluted samples (typically 50–100 µg total protein per well for colon lysates) and incubated for 2 h at room temperature. After washing away unbound material, biotinylated detection antibodies were applied, followed by horseradish peroxidase (HRP)-conjugated streptavidin. A 3,3′,5,5′-tetramethylbenzidine (TMB) substrate solution was added and allowed to develop for 10–20 min, then the reaction was stopped with 2 N H2SO4. Absorbance was measured at 450 nm (with a 570 nm reference) using a microplate reader. Cytokine concentrations in the samples (pg/mL) were determined by interpolating from a standard curve generated with known concentrations of recombinant cytokines. Finally, cytokine levels were normalized to the total protein content of each sample and reported as pg cytokine per mg tissue protein. Each sample was assayed in duplicate. The ELISAs had detection sensitivities in the range of tens of pg/mL, and all measured values fell within the linear range of the assays after appropriate dilution.

Naive CD4$^+$ T Cell Isolation and Culture

To examine T cell differentiation, naive CD4$^+$ T cells were isolated from the spleens of WT and PTPRO$^{-/-}$ mice and cultured under defined polarization conditions. Spleens were mechanically dissociated through a 70 µm cell strainer to obtain single-cell suspensions, and red blood cells were lysed using an ammonium chloride buffer. Naive CD4$^+$ T cells were then enriched by magnetic negative selection (Naive CD4$^+$ T Cell Isolation Kit; 8804-6824-74, Thermo Fisher Scientific, Waltham, MA, USA). Flow cytometry confirmed that the isolated CD4$^+$ T cell populations were >95% pure.

Cells were cultured in complete RPMI-1640 medium (11875093, Gibco, Thermo Fisher Scientific, Waltham, MA, USA) supplemented with 10% heat-inactivated fetal bovine serum (FBS), 100 U/mL penicillin, 100 µg/mL streptomycin, and 50 µM β-mercaptoethanol. To polyclonally activate the T cells, plate-bound anti-CD3 (2 µg/mL) and soluble anti-CD28 (1 µg/mL) antibodies (MA5-16623, 14-0281-82, both from eBioscience, Thermo Fisher Scientific, Waltham, MA, USA) were added to the cultures. Cells were maintained at 37 °C in a humidified 5% CO_2 incubator.

Two T cell polarization conditions were set up in parallel: one promoting Th1 differentiation and one promoting Treg differentiation. For Th1-skewing, we added recombinant mouse IL-12 (20 ng/mL; 210-12-50UG, PeproTech, Rocky Hill, NJ, USA) at culture initiation to drive Th1 lineage commitment, and included a neutralizing anti–IL-4 antibody (10 µg/mL; HY-P990121, MedChemExpress, Monmouth Junction, NJ, USA) to prevent Th2 deviation. For Treg-skewing, we supplemented the cultures with transforming growth factor-β (TGF-β, 5 ng/mL; 100-21C-50UG, PeproTech, Rocky Hill, NJ, USA) in addition to IL-12. The presence of TGF-β favors the development of inducible Foxp3$^+$ Tregs even alongside IL-12, creating a mixed polarization environment to reveal any intrinsic bias between WT and PTPRO$^{-/-}$ T cells. Cultures were maintained for up to 6 days; on day 3, fresh medium containing the same cytokines was added to support cell viability and polarization signals. On day 6, cells were harvested for analysis.

For flow cytometric analysis of intracellular markers (IFN-γ, TNF-α, and Foxp3), a subset of cells was restimulated during the final 4–6 h of culture with phorbol 12-myristate 13-acetate (PMA, 50 ng/mL) and ionomycin (1 µg/mL) in the presence of GolgiStop/GolgiPlug (554724, BD Biosciences, San Jose, CA, USA) to block cytokine secretion. Parallel cell samples were collected without restimulation for mRNA extraction. Each experimental condition (Th1 or Treg polarization) was set up in triplicate wells for both WT and PTPRO$^{-/-}$ cells. Experiments were repeated using cells from at least 3–4 different mice per genotype to ensure the results were reproducible [26].

Flow Cytometry

Flow cytometry was employed to identify and quantify Th1 and Treg cell populations in both colonic tissues and the *in vitro* T cell cultures. For lamina propria lymphocyte isolation from the colon, freshly harvested colonic tissue was washed and cut into small pieces, then incubated in Hanks' balanced salt solution (HBSS) containing 5 mM ethylene diamine tetraacetic acid (EDTA) and 1mM dithiothreitol (DTT) at 37 °C to strip away the epithelial layer. The remaining tissue fragments were digested with collagenase VIII (1 mg/mL; C2139, Sigma-Aldrich, St. Louis, MO, USA) and DNase I (100 µg/mL) for 40 min at 37 °C with gentle agitation. The resulting cell suspension was filtered through a cell strainer, washed, and then subjected to a two-step Percoll gradient (40%/80%) centrifugation to enrich mononuclear cells. Cells at the 40/80% interface (lamina propria lymphocytes) were collected for staining. (For spleen cells or cultured T cells, single-cell suspensions were prepared as described above).

Surface and intracellular staining were performed using fluorochrome-conjugated monoclonal antibodies. To analyze Th1 cells, we stained cells for surface CD4 and intracellular Th1 cytokines. Specifically, cells were first incubated with a fluorescently labeled anti-CD4 antibody (e.g., CD4-PerCP-Cy5.5, clone GK1.5) for 30 min at 4 °C in fluorescence-activated cell sorting (FACS) buffer (PBS + 2% FBS) to label CD4$^+$ T cells. After fixation and permeabilization (Foxp3/Transcription Factor Staining Buffer Set, 00-5523-00, eBioscience, Thermo Fisher Scientific, Waltham, MA, USA), cells were stained intracellularly with anti–IFN-γ (APC conjugate, clone XMG1.2, 17-7311-82, eBioscience, Thermo Fisher Scientific, Waltham, MA, USA) and anti–TNF-α (PE conjugate, clone MP6-XT22, 14-7321-81, eBioscience, Thermo Fisher Scientific, Waltham, MA, USA) antibodies. For Treg identification, surface CD4 staining was performed similarly, and after permeabilization, cells were stained with anti-Foxp3 (Alexa Fluor 488, clone FJK-16s, 53-5773-82, eBioscience, Thermo Fisher Scientific, Waltham, MA, USA) and anti–IL-10 (PE, clone JES5-16E3, 12-7101-82, eBioscience, Thermo Fisher Scientific, Waltham, MA, USA) antibodies. Appropriate isotype-matched control antibodies were included to set gating thresholds. In some experiments, additional markers such as anti-CD25 and anti-CD69 were used to assess T cell activation, and a viability dye was added to exclude dead cells.

Stained samples were acquired on a flow cytometer (either BD FACSCanto II, BD Biosciences, San Jose, CA, USA or Beckman Coulter CytoFLEX, Beckman Coulter, Brea, CA, USA). Compensation settings were determined using single-color controls. For each sample, 50,000–100,000 events in the lymphocyte gate were recorded. Data were analyzed using FlowJo v10.6.1 software (Tree Star, Ashland, OR, USA). The gating strategy was: first, singlets (FSC-H vs. FSC-A) were gated; next, lymphocytes were gated by FSC vs. SSC; then live cells were gated by excluding dead cells (viability dye positive); finally, CD4$^+$ T cells were gated. Th1 cells were defined as CD4$^+$ cells positive for IFN-γ and/or TNF-α. Tregs were defined as CD4$^+$ Foxp3$^+$ cells, and we also noted the subset of Foxp3$^+$ cells that produced IL-10. Flow cytometry data are expressed as the percentage of positive cells within the CD4$^+$ gate. In the figures, group results are presented as mean ± SD for n = 6 mice per group (or n = 6 independent culture replicates) with appropriate statistical comparisons.

For intracellular phospho-flow cytometry (used to assess signaling in certain *in vitro* assays with recombinant PTPRO, see Results), cells were fixed with 4% paraformaldehyde at 37 °C for 10 min, then permeabilized with ice-cold methanol for 30 min. Cells were subsequently stained with antibodies against Phospho-JAK2 (Tyr1007, Tyr1008) (APC conjugate, MA5-37199, Invitrogen, Thermo Fisher Scientific, Waltham, MA, USA) or Phospho-STAT5 (Tyr694) (APC conjugate, 17-9010-42, eBioscience, Thermo Fisher Scientific, Waltham, MA, USA), along with surface CD4-PE, and then analyzed by flow cytometry. Mean fluorescence intensity (MFI) val-

ues for phosphorylated JAK2 (p-JAK2) and phosphorylated STAT5 (p-STAT5) were quantified.

Western Blotting

Total protein lysates were prepared from colon tissues or cultured T cells using radioimmunoprecipitation assay (RIPA) buffer (50 mM Tris-HCl pH 7.5, 150 mM NaCl, 1% NP-40, 0.5% sodium deoxycholate, 0.1% SDS) supplemented with protease and phosphatase inhibitor cocktails (Roche Complete Mini and PhosSTOP, 11836170001, Roche Diagnostics GmbH, Mannheim, Baden-Württemberg, Germany). Lysates were incubated on ice for 30 min, then centrifuged at 14,000 $\times$g for 15 min at 4 °C. The clarified supernatants were collected and protein concentrations were determined by BCA assay. For each sample, 30–50 µg of protein was mixed with SDS sample loading buffer and boiled for 5 min. Proteins were separated on 8–12% sodium dodecyl sulfate-polyacrylamide gel electrophoresis (SDS-PAGE) and transferred onto polyvinylidene fluoride (PVDF) membranes (IPVH00010, MilliporeSigma, Burlington, MA, USA). Membranes were blocked at room temperature for 1 h in TBST (TBS + 0.1% Tween-20), containing 5% non-fat milk. Blots were then incubated overnight at 4 °C with primary antibodies. The primary antibodies used were: anti-PTPRO (mouse monoclonal; 67000-1-Ig, Proteintech, Wuhan, China; 1:1000), anti-JAK2 (rabbit polyclonal; 17670-1-AP, Proteintech, Wuhan, China; 1:1000), anti–phospho-JAK2 (Tyr1007/1008) (rabbit polyclonal; ab32101, Abcam, Cambridge, UK; 1:1000), anti-STAT5 (rabbit monoclonal; 9363, Cell Signaling Technology, Danvers, MA, USA; 1:1000), anti–phospho-STAT5 (Tyr694) (rabbit monoclonal; 9359, Cell Signaling Technology, Danvers, MA, USA; 1:1000), and anti–β-actin (mouse monoclonal; 60008-1-Ig, Proteintech, Wuhan, China; 1:5000). After the primary antibody incubation, membranes were washed three times with TBST and then incubated for 1 h at room temperature with the appropriate HRP–conjugated secondary antibody (goat anti-mouse immunoglobulin G (IgG)-HRP or goat anti-rabbit IgG-HRP; 111-005-003, 115-005-003, Jackson ImmunoResearch, West Grove, PA, USA; 1:5000). Blots were washed again, and immunoreactive bands were visualized using an enhanced chemiluminescence (ECL) substrate (Clarity Western ECL kit, 1705060, Bio-Rad, Hercules, CA, USA) and captured on a chemiluminescent imaging system.

For quantification, blot images were scanned and measured in band intensities using ImageJ v1.54i software (National Institutes of Health, Bethesda, MD, USA). The intensity of phosphorylated protein bands was normalized to the corresponding total protein band (e.g., p-STAT5 normalized to total STAT5), and total protein bands were normalized to β-actin as a loading control. Normalized results were expressed as relative intensity (fold-change) compared to control samples. Each western blot analysis was performed on at least three independent biological samples per group. In the figures, representative blot images are shown alongside pooled densitometry data (mean $\pm$ SD).

Co-Immunoprecipitation (Co-IP)

Co-IP assays were performed to determine whether PTPRO and JAK2 physically interact in colon tissue. Approximately 100 mg of colon tissue from DSS-treated WT mice was homogenized in NP-40 lysis buffer (20 mM Tris-HCl pH 7.5, 150 mM NaCl, 1% NP-40, 10% glycerol) supplemented with protease and phosphatase inhibitors. To pre-clear the lysate, 500 µg of the clarified supernatant was incubated with 20 µL of Protein A/G agarose beads (sc-2003, Santa Cruz Biotechnology, Dallas, TX, USA) for 1 h at 4 °C, to remove proteins that bind nonspecifically to the beads. The pre-cleared supernatant was then split into aliquots and incubated overnight at 4 °C with one of the following antibodies: 2 µg of anti-PTPRO (67000-1-Ig, Proteintech, Wuhan, China), 2 µg of anti-JAK2 (17670-1-AP, Proteintech, Wuhan, China), or 2 µg of an isotype-matched control IgG (negative control).

Immune complexes were captured by adding 30 µL of Protein A/G agarose beads and rotating for 2 h at 4 °C. The beads were then washed four times with cold lysis buffer to remove unbound proteins. Bound proteins were eluted by boiling the beads in SDS sample buffer. The resulting immunoprecipitates were analyzed by western blot as described above. Blots were probed with anti-JAK2 and anti-PTPRO antibodies to determine if each protein co-precipitated with the other. Successful co-immunoprecipitation was indicated by detection of JAK2 in the PTPRO IP sample and detection of PTPRO in the JAK2 IP sample, while neither was present in the IgG control IP. These Co-IP experiments were repeated at least twice with similar results.

Statistical Analysis

All quantitative results are reported as mean $\pm$SD. Statistical analyses were carried out using GraphPad Prism version 9.5.0 (GraphPad Software, San Diego, CA, USA). The normality of the data was assessed using the Shapiro–Wilk test. For data that met the assumptions of normality, an unpaired two-tailed Student's *t*-test was used for comparisons between two groups (e.g., WT vs. PTPRO$^{-/-}$ under one condition). For comparisons among multiple groups (more than two genotypes or treatment conditions), one-way analysis of variance (ANOVA) was applied, followed by Tukey's *post hoc* test for pairwise comparisons. For repeated measures such as body weight over time, a two-way repeated-measures ANOVA was performed with Bonferroni's *post hoc* correction. For data that did not meet the assumption of normality, Welch's ANOVA test was used for multiple comparisons, followed by Dunnett's post hoc test. For two-group comparisons with non-normal data, the Mann-Whitney U test was used. A p value < 0.05 was con-

sidered statistically significant. All experiments were conducted at least twice independently to ensure reproducibility. Mice were allocated to experimental groups based on genotype and treatment (randomization was not applicable beyond these criteria). Investigators were blinded to group assignments during histological scoring and flow cytometry analysis to reduce bias.

Results

PTPRO Expression Is Upregulated in Ulcerative Colitis

To investigate the potential involvement of PTPRO in UC pathogenesis, we first examined PTPRO expression in ulcerative colitis to determine whether its levels correlate with disease activity. In the DSS-induced acute colitis mouse model (Fig. 1A), PTPRO expression was markedly elevated in inflamed colonic tissues compared to healthy controls. Colonic samples from DSS-treated mice exhibited significantly higher *PTPRO* mRNA levels (~3–4-fold increase) relative to untreated mice ($p < 0.05$ by RT-qPCR; Fig. 1B). At the protein level, western blot analysis corroborated this upregulation: PTPRO band intensity in colon lysates from DSS-treated mice was several-fold higher than in control mice (normalized to β-actin; Fig. 1C). Densitometry analysis revealed that PTPRO protein levels in DSS colitis were approximately 2.5 times those in controls ($p < 0.05$).

We next examined PTPRO expression in colon biopsy specimens from UC patients. *PTPRO* mRNA in colonic biopsies was low or undetectable in healthy individuals, whereas it was significantly elevated in patients with active UC (Fig. 1D). Importantly, PTPRO expression levels correlated with disease severity. Patients with moderate-to-severe UC had substantially higher *PTPRO* mRNA levels (approximately 2–4-fold above normal controls, $p < 0.05$) than patients with quiescent or mild disease. In contrast, patients with mild UC showed only a slight, non-significant increase in PTPRO expression compared to controls. Western blot analysis demonstrated that colonic samples from moderate-to-severe UC patients displayed stronger PTPRO protein bands (normalized to β-actin) compared to healthy colon samples (Fig. 1E, left). Quantification confirmed that PTPRO protein was significantly upregulated in severe UC (Fig. 1E, right). Collectively, these data indicate that PTPRO expression is elevated during active colitis in both murine models and human disease. Moreover, the positive correlation between PTPRO levels and UC severity suggests that PTPRO may contribute to the inflammatory process in UC.

PTPRO Deficiency Ameliorates DSS-Induced Colitis

To assess the functional impact of PTPRO on colitis, we compared DSS-induced disease outcomes in PTPRO$^{-/-}$ mice versus WT mice (Fig. 2A). Striking differences emerged, suggesting that PTPRO deficiency confers protection against DSS-induced colonic inflammation. Both WT and PTPRO$^{-/-}$ mice began losing weight around days 3–4 of DSS exposure, but the PTPRO$^{-/-}$ mice lost significantly less weight over time (Fig. 2B). By day 12, WT mice had lost ~15–20% of their starting body weight, whereas PTPRO$^{-/-}$ mice lost only ~5–10% ($p < 0.05$). This divergence in weight loss was statistically significant by day 6 and persisted through day 12, consistent with a milder disease course in PTPRO-deficient animals. Consistent with these observations, the DAI—a composite score of weight loss, diarrhea, and bleeding—was markedly lower in PTPRO$^{-/-}$ mice than in WT mice. By day 12, WT mice had a mean DAI of ~8–9 (on a 0–12 scale), indicating severe colitis, whereas PTPRO$^{-/-}$ mice had a mean DAI of ~5–6, indicating only mild disease (Fig. 2C). The difference in DAI between genotypes was highly significant ($p < 0.05$). Notably, throughout DSS treatment, PTPRO$^{-/-}$ mice exhibited firmer stools and less fecal bleeding than WT mice, consistent with their attenuated colitis symptoms. Macroscopic examination at necropsy supported these findings of disease amelioration in PTPRO$^{-/-}$ mice. DSS-treated WT mice exhibited the expected phenotype of shortened, inflamed colons (mean length ~4.2 cm vs. ~6.5 cm in untreated healthy mice). In contrast, compared with the DSS-treated WT mice, the colons were visibly longer and less edematous after DSS in PTPRO$^{-/-}$ mice (Fig. 2D). Measurement of colon length revealed that PTPRO$^{-/-}$ colons were on average 1.5–2 cm longer than WT colons following DSS ($p < 0.05$), nearly approaching the length of normal colons. This finding suggests that the absence of PTPRO reduces colonic shortening (and thus tissue damage and fibrosis) during colitis. Histopathological examination of colon tissues confirmed that PTPRO$^{-/-}$ mice sustained far less damage than WT mice (Fig. 2E). DSS-treated WT colons showed dense inflammatory infiltrates throughout the mucosa and submucosa, goblet cell depletion, thickened colonic walls, crypt abscesses, and deep epithelial ulcerations (Fig. 2E). By contrast, DSS-treated PTPRO$^{-/-}$ colons retained relatively intact crypt architecture and had markedly fewer inflammatory cells (Fig. 2E). The inflammation that was present in PTPRO$^{-/-}$ mice was mostly superficial and localized, with large areas of epithelium remaining intact (Fig. 2E). Accordingly, aggregate histology scores were significantly lower for PTPRO$^{-/-}$ mice (Fig. 2F). On the 0–12 scale, WT mice scored ~7–8 (severe inflammation and ulceration), whereas PTPRO$^{-/-}$ mice scored ~4–5 (mild inflammation) (Fig. 2F). At the molecular level, the absence of PTPRO was associated with a blunted inflammatory response in the colon. We assessed colonic pro-inflammatory cytokine levels by RT-qPCR. In DSS-treated WT mice, transcripts for *TNF-α* and *IL-6* were greatly elevated, reflecting active inflammation (Fig. 2G,H). Strikingly, the colonic *TNF-α* and *IL-6* mRNA levels in the DSS-treated PTPRO$^{-/-}$ group

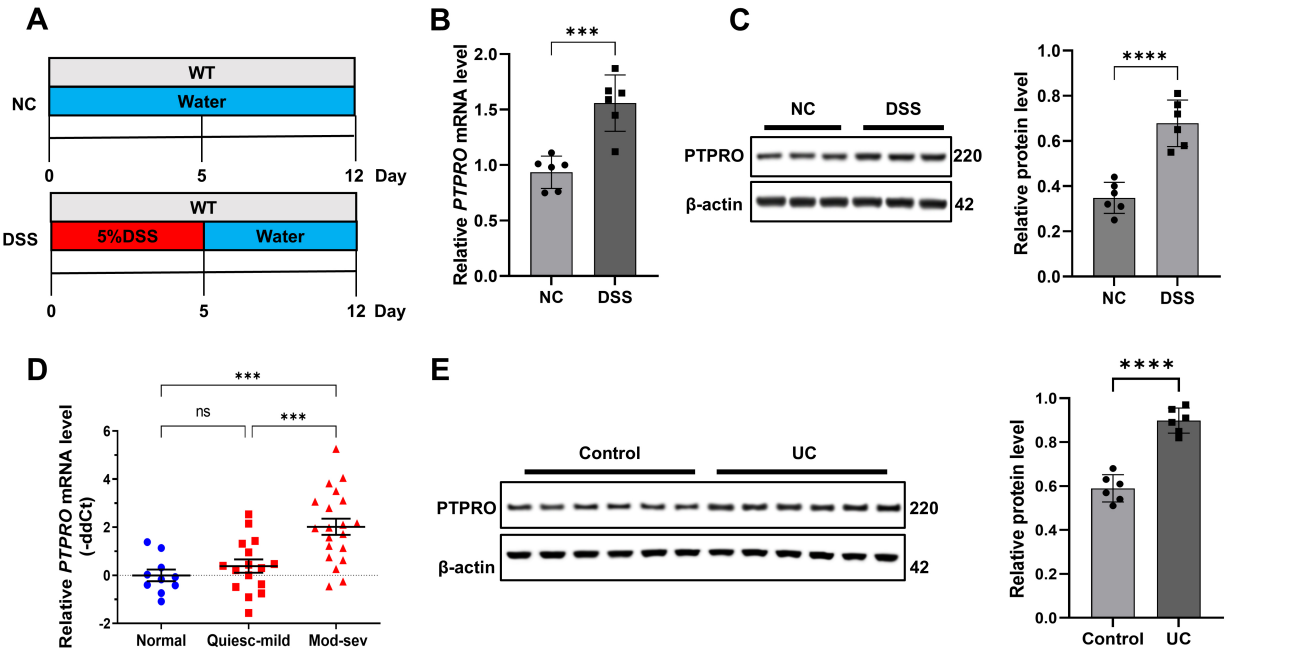

Fig. 1. PTPRO expression is elevated in ulcerative colitis mice and patients. (A) Schematic diagram of the ulcerative colitis model induction. WT mice aged 6–8 weeks were administered drinking water containing 5% (w/v) DSS for 5 days, followed by normal water for 7 days. The normal control (NC) group mice received normal drinking water for 12 days. (B) Detection of *PTPRO* mRNA expression in mouse colon tissues by RT-qPCR. Data are expressed as fold change relative to the NC group. n = 6 mice per group. (C) Representative western blot images (top) and densitometric quantification (bottom) showing PTPRO protein expression in colon tissues from NC and DSS groups. PTPRO protein levels were normalized to β-actin. Numbers indicate molecular weight in kDa. n = 6 mice per group. (D) Detection of *PTPRO* mRNA expression in colon tissues from normal individuals (n = 10), quiescent-mild UC patients (Quiesc-mild, n = 16), and moderate-severe UC patients (Mod-sev, n = 20) by RT-qPCR. Data are expressed as fold change relative to normal controls. Each dot represents one patient. (E) Representative western blot images (left) and densitometric quantification (right) showing PTPRO protein expression in colon tissues from healthy controls and moderate-severe UC patients. PTPRO protein levels were normalized to β-actin. Numbers indicate molecular weight in kDa. n = 6 samples per group. Data are expressed as mean ± SD. ***$p < 0.001$; ****$p < 0.0001$. For (B) and (C), an unpaired two-tailed Student's *t*-test was used for statistical analysis; for (D) and (E), one-way ANOVA followed by Tukey post-hoc test was performed. PTPRO, protein tyrosine phosphatase receptor-type O; WT, wild-type; DSS, dextran sulfate sodium; RT-qPCR, real-time quantitative polymerase chain reaction; UC, ulcerative colitis; ANOVA, one-way analysis of variance; ns, not significant.

were approximately 50% lower than in the DSS-treated WT group (Fig. 2G,H). These data suggest that the typical inflammatory "cytokine storm" of DSS colitis is substantially dampened in the absence of PTPRO. Another hallmark of DSS colitis is goblet cell loss and mucus depletion, which compromise the mucosal barrier. We performed AB/PAS staining to examine goblet cells in colon crypts. As expected, DSS-treated WT mice showed severe goblet cell depletion—only a few mucus-producing goblet cells (purple-stained) remained in the damaged epithelium (Fig. 2I). In contrast, PTPRO$^{-/-}$ mice retained far more goblet cells per crypt, indicating preservation of mucosal secretory function (Fig. 2I). Quantification showed that WT mice had on average only 110 goblet cells per field after DSS, whereas PTPRO$^{-/-}$ mice had about 210 goblet cells per field—nearly normal levels ($p < 0.05$ vs. WT-DSS; Fig. 2J). Thus, PTPRO deficiency protected against goblet cell loss and helped maintain the colonic mucus layer. Collectively, these results demonstrate that PTPRO$^{-/-}$ mice are markedly protected from DSS-induced colitis. They experience milder clinical signs, less weight loss, and minimal histological damage compared to WT mice. PTPRO$^{-/-}$ mice also exhibit a dampened pro-inflammatory cytokine profile and preservation of goblet cells. These findings implicate PTPRO as a pro-inflammatory factor in colitis, such that its absence produces an anti-inflammatory, tissue-protective effect.

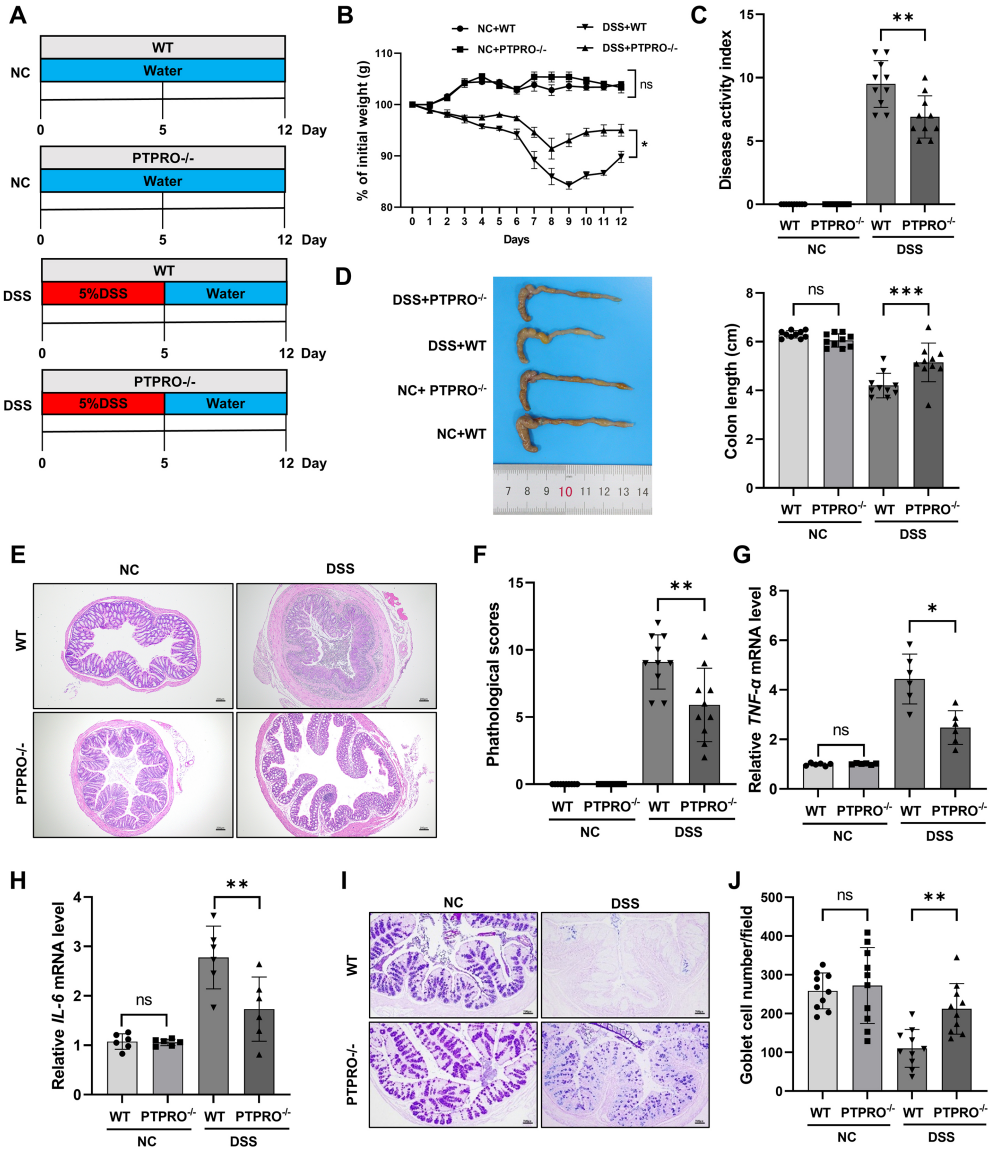

Fig. 2. PTPRO knockout ameliorates ulcerative colitis in mice. (A) Experimental design schematic for panels (B–J). WT and PTPRO$^{-/-}$ mice were assigned to NC or DSS treatment groups. In DSS groups, mice received drinking water containing 5% (w/v) DSS from day 0 to day 5, followed by normal water for 7 days. NC groups received normal drinking water throughout the 12-day period. (B) Body weight changes in mice during the experimental period. Data are expressed as percentage of initial body weight. n = 10 mice per group. (C) DAI scores measured on day 12. DAI was calculated as the sum of weight loss, stool consistency, and rectal bleeding scores. n = 10 mice per group. (D) Representative images of colon tissues from each experimental group (left) and quantification of colon length (right). Scale bar represents 1 cm. n = 10 mice per group. (E) Representative H&E staining images of distal colon from NC and DSS groups in WT and PTPRO$^{-/-}$ mice. Scale bar, 200 μm. (F) Histopathological scores evaluating inflammation severity, tissue damage, and architectural distortion. n = 10 mice per group. (G,H) Detection of *TNF-α* (G) and *IL-6* (H) mRNA expression levels in mouse colon tissues by RT-qPCR. Data are expressed as fold change relative to the NC + WT group. n = 6 mice per group. (I) Representative AB/PAS staining images showing goblet cells (purple-stained) in colon crypts from each experimental group. Scale bar, 100 μm. (J) Quantification of goblet cell numbers per field. At least 20 well-oriented crypts were counted per mouse. n = 10 mice per group. Data are expressed as mean ± SD. *$p < 0.05$; **$p < 0.01$; ***$p < 0.001$. For (B), two-way ANOVA with repeated measures followed by Bonferroni post-hoc test was performed; for (C), (D), (F), (G), (H), and (J), one-way ANOVA followed by Tukey post-hoc test was used for statistical analysis. PTPRO$^{-/-}$, PTPRO knockout; AB/PAS, Alcian Blue/Periodic Acid-Schiff; TNF-α, tumor necrosis factor-α; IL-6, interleukin-6; H&E, hematoxylin and eosin; DAI, Disease Activity Index.

PTPRO Knockout Restores Intestinal Immune Homeostasis by Modulating Th1/Treg Balance

To investigate how PTPRO deficiency leads to reduced inflammation, we focused on the Th1/Treg axis known to be dysregulated in UC. We examined whether loss of PTPRO alters the mucosal immune profile, especially the balance of $CD4^+$ T cell subsets. We first profiled key pro- and anti-inflammatory mediators in the colon. In DSS-colitic WT mice, the levels of Th1-associated cytokines IFN-γ, TNF-α, IL-6, and IL-1β levels in colon tissue were all significantly elevated compared to the NC + WT group. However, these cytokines were markedly reduced in the DSS + $PTPRO^{-/-}$ group compared with the DSS + WT group. For example, $PTPRO^{-/-}$ colons produced approximately 40–50% less IFN-γ and TNF-α than WT colons following DSS treatment ($p < 0.05$), and IL-6 and IL-1β were also substantially reduced (Fig. 3A). Notably, IL-10—a key Treg-associated anti-inflammatory cytokine—was approximately two-fold higher in $PTPRO^{-/-}$ colons than in WT colons ($p < 0.05$), indicating a shift toward an immunoregulatory environment. We also measured *Foxp3* gene expression as a proxy for Treg abundance. By RT-qPCR (Fig. 3B), *Foxp3* mRNA in DSS-treated $PTPRO^{-/-}$ mice was 2–3 times higher than in DSS-treated WT mice ($p < 0.05$), consistent with an expanded Treg compartment. The qPCR data showed that *IFN-*γ, *TNF-*α, *IL-6*, and *IL-1*β were also significantly lower in $PTPRO^{-/-}$ vs. WT colitis (Fig. 3B), whereas *IL-10* was higher, corroborating the protein data. Taken together, these results suggest that deleting PTPRO skews the colonic cytokine milieu away from pro-inflammatory signals and toward anti-inflammatory ones.

To directly examine T cell subsets, we performed flow cytometry on lamina propria lymphocytes from the colons of DSS-treated mice. Live $CD4^+$ T cells were gated and analyzed for intracellular IFN-γ and TNF-α to identify Th1 cells, and for intracellular Foxp3 (with IL-10 co-staining) to identify Tregs (Fig. 3C,D). This analysis revealed a pronounced rebalancing of T helper subsets in $PTPRO^{-/-}$ mice. In DSS-treated WT colons, Th1 cells were highly enriched: approximately 15–20% of $CD4^+$ T cells were IFN-γ+ (compared to <5% in healthy colons). In DSS-treated $PTPRO^{-/-}$ colons, however, Th1 cells were significantly reduced. Only ~8–10% of $CD4^+$ T cells in $PTPRO^{-/-}$ mice were IFN-γ^+, approximately half the frequency observed in WT mice ($p < 0.05$; Fig. 3C). A similar reduction was seen in TNF-α^+ $CD4^+$ cells, indicating an overall decrease in Th1 effector T cells in PTPRO-deficient colons.

Moreover, compared with the NC + WT group, $Foxp3^+$ $CD4^+$ cells were significantly reduced in DSS + WT mice. However, the Treg population in DSS + $PTPRO^{-/-}$ mice was markedly restored relative to the DSS + WT group (Fig. 3D). Moreover, a substantial subset of these Tregs in $PTPRO^{-/-}$ mice co-expressed IL-10, consistent with a highly suppressive phenotype. $Foxp3^+$ IL-10+ Tregs were approximately twice as frequent in $PTPRO^{-/-}$ colons as in WT colons (Fig. 3D, right panel). This increased Treg representation in $PTPRO^{-/-}$ mice aligns with their elevated Foxp3 mRNA and IL-10 levels noted above.

In summary, PTPRO deficiency shifts the colonic Th1/Treg balance toward Tregs. This reduces Th1 cells and increases mucosal Tregs. This immune rebalancing—characterized by reduced IFN-γ/TNF-α and increased IL-10/Foxp3—provides a plausible explanation for the milder colitis observed in $PTPRO^{-/-}$ mice. By tipping the scales toward anti-inflammatory Treg activity and away from pathogenic Th1 responses, PTPRO knockout mice achieve a state of improved intestinal immune homeostasis, thereby mitigating colitis severity.

PTPRO Deficiency Suppresses Th1 Differentiation and Enhances Treg Induction In Vitro

Our *in vivo* findings suggested that PTPRO intrinsically promotes pro-inflammatory Th1 responses while restraining Treg development. To test this hypothesis directly, we carried out *in vitro* polarization assays with naive $CD4^+$ T cells from WT and $PTPRO^{-/-}$ mice. This approach allowed us to observe T cell fate decisions in a controlled environment, isolated from the complexities of *in vivo* immunity.

We cultured naive $CD4^+$ T cells under two sets of conditions: Th1-polarizing (with IL-12) and Treg-inducing (with IL-12 + TGF-β). After 5–6 days of culture, cells were analyzed by flow cytometry for Th1 and Treg markers (Fig. 4). Under Th1-polarizing conditions (IL-12 with anti-CD3/anti-CD28, without exogenous TGF-β), WT $CD4^+$ T cells readily differentiated into Th1 effectors. A substantial fraction of WT cells became IFN-γ^+ (~30%) and TNF-α^+, indicative of strong Th1 lineage commitment (Fig. 4A). $Foxp3^+$ Tregs remained very low (~5%) in the absence of TGF-β, with no significant difference between WT and $PTPRO^{-/-}$ groups (Fig. 4A). In contrast, $PTPRO^{-/-}$ $CD4^+$ T cells showed a reduced propensity for Th1 differentiation under the same conditions. The proportion of IFN-γ^+ $CD4^+$ T cells in $PTPRO^{-/-}$ cultures was significantly lower than in WT cultures (~20% vs ~30%, $p < 0.05$; Fig. 4A). Likewise, the frequency of TNF-α^+ $CD4^+$ cells was decreased in $PTPRO^{-/-}$ cultures (Fig. 4A). Thus, without PTPRO, naive T cells were less efficient at adopting a Th1 phenotype even under strong IL-12 stimulation.

We next evaluated T cell differentiation under conditions including TGF-β, which provides a potent Foxp3 induction signal even in an IL-12-rich environment. In WT cultures, adding TGF-β led to the emergence of a sizeable Treg population (~25% $Foxp3^+$ cells among $CD4^+$ cells) while still allowing some Th1 development (~10% IFN-γ^+ cells) (Fig. 4B). Remarkably, $PTPRO^{-/-}$ T cells displayed dramatically enhanced Treg differentiation under these IL-12 + TGF-β conditions. In $PTPRO^{-/-}$ cultures, $Foxp3^+$ T cells constituted ~30–40% of $CD4^+$ cells,

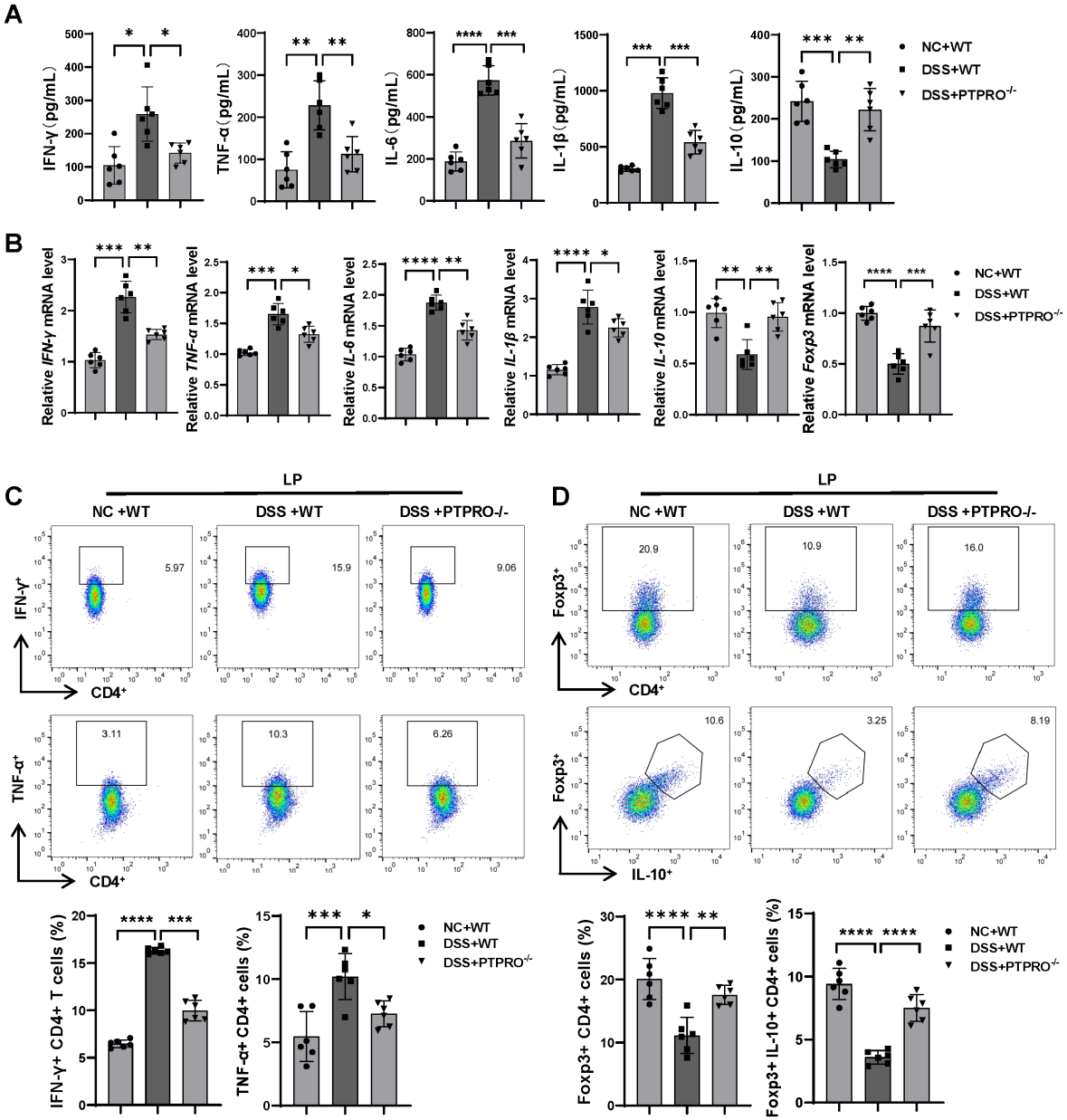

Fig. 3. PTPRO knockout shapes intestinal immune responses by regulating regulatory T cell (Treg)/helper T cell 1 (Th1) balance. WT and PTPRO$^{-/-}$ mice were assigned to NC or DSS treatment groups. In DSS groups, mice received drinking water containing 5% (w/v) DSS from day 0 to day 5, followed by normal water for 7 days. NC groups received normal drinking water for 12 days. (A) Detection of IFN-γ, TNF-α, IL-6, IL-1β, and IL-10 protein levels in colon tissue homogenates by ELISA. Data are expressed as pg/mg protein. n = 6 mice per group. (B) Detection of *IFN-γ*, *TNF-α*, *IL-6*, *IL-1β*, *IL-10*, and *Foxp3* mRNA expression levels in mouse colon tissues by RT-qPCR. Data are expressed as fold change relative to the NC + WT group. n = 6 mice per group. (C) Flow cytometry analysis of Th1 cell subsets in colon lamina propria (LP) cells. Representative flow cytometry plots (top) and quantitative analysis (bottom) showing IFN-γ^+ CD4$^+$ T cells and TNF-α^+ CD4$^+$ T cells. Cells were gated on live CD4$^+$ T cells, and percentages indicate positive cells within the CD4$^+$ gate. n = 6 mice per group. (D) Flow cytometry analysis of Treg cell subsets in colon LP cells. Representative flow cytometry plots (top) and quantitative analysis (bottom) showing Foxp3$^+$ CD4$^+$ T cells and Foxp3$^+$ IL-10$^+$ T cells. Cells were gated on live CD4$^+$ T cells, and percentages indicate positive cells within the CD4$^+$ gate. n = 6 mice per group. Data are expressed as mean ± SD. *$p < 0.05$; **$p < 0.01$; ***$p < 0.001$; ****$p < 0.0001$. For all panels, one-way ANOVA followed by Tukey post-hoc test was performed for statistical analysis. ELISA, enzyme-linked immunosorbent assay; IFN-γ, interferon-γ; IL-1β, interleukin-1β; IL-10, interleukin-10; Foxp3, Forkhead box P3; CD4, clusters of differentiation 4.

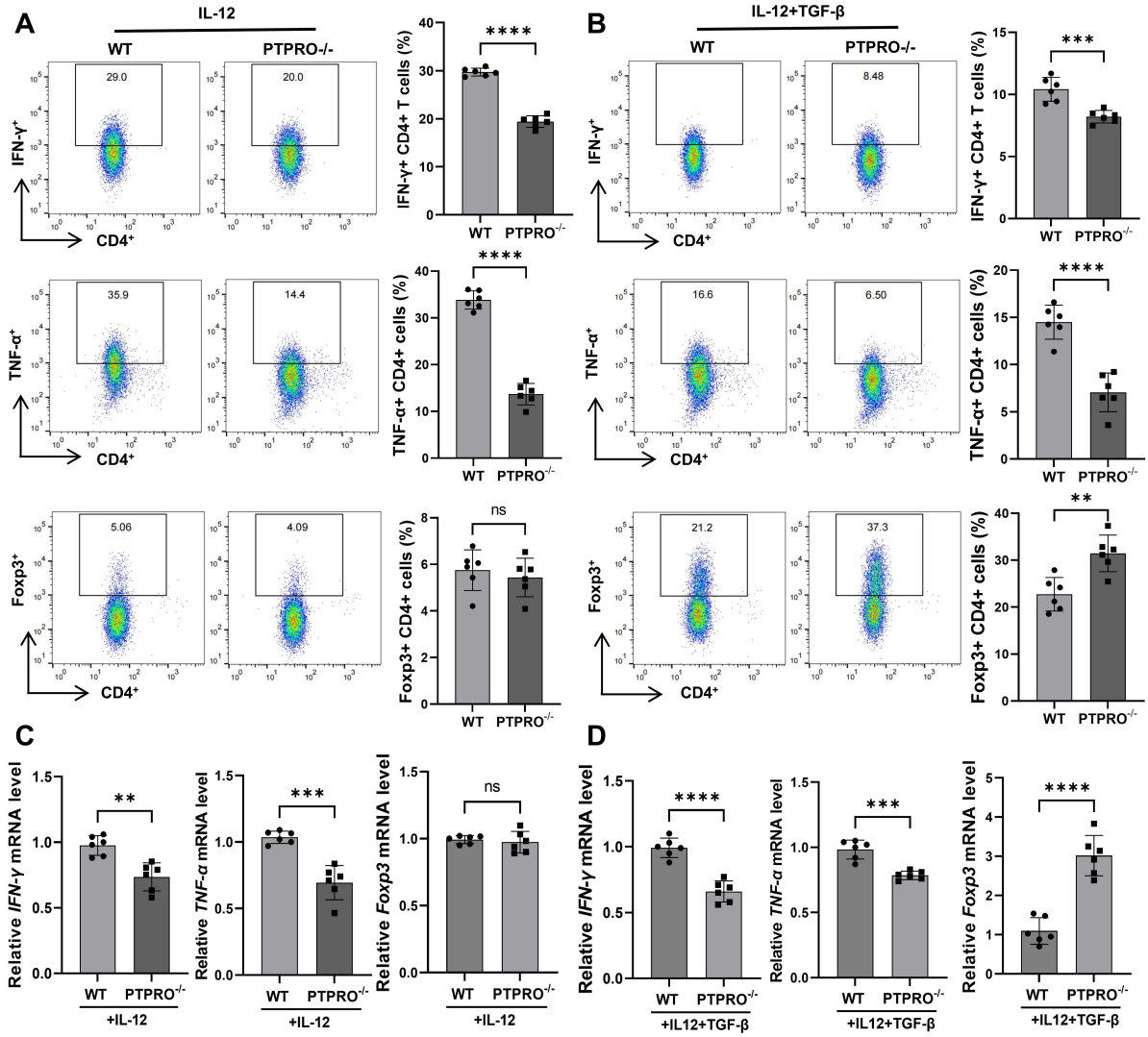

Fig. 4. PTPRO knockout inhibits Th1 and promotes Treg cell differentiation *in vitro*. Native $CD4^+$ T cells were isolated from spleens of WT and $PTPRO^{-/-}$ mice using anti-mouse native CD4 magnetic beads and activated *in vitro* with anti-CD3 and anti-CD28 antibodies for 72 h. (A) Flow cytometry analysis of T cell differentiation under IL-12 polarization conditions (20 ng/mL IL-12). Representative flow cytometry plots (left) and quantitative analysis (right) showing IFN-γ^+ $CD4^+$ T cells, TNF-α^+ $CD4^+$ T cells, and $Foxp3^+$ $CD4^+$ T cells. Cells were gated on live $CD4^+$ T cells, and percentages indicate positive cells within the $CD4^+$ gate. n = 6 independent experiments. (B) Flow cytometry analysis of T cell differentiation under combined IL-12 and TGF-β polarization conditions (20 ng/mL IL-12 + 5 ng/mL TGF-β). Representative flow cytometry plots (left) and quantitative analysis (right) showing IFN-γ^+ $CD4^+$ T cells, TNF-α^+ $CD4^+$ T cells, and $Foxp3^+$ $CD4^+$ T cells. Cells were gated on live $CD4^+$ T cells, and percentages indicate positive cells within the $CD4^+$ gate. n = 6 independent experiments. (C) Detection of *IFN-*γ, *TNF-*α, and *Foxp3* mRNA expression levels by RT-qPCR in native $CD4^+$ T cells cultured under IL-12 polarization conditions. Data are expressed as fold change relative to the WT + IL-12 group. n = 6 independent experiments. (D) Detection of *IFN-*γ, *TNF-*α, and *Foxp3* mRNA expression levels by RT-qPCR in native $CD4^+$ T cells cultured under IL-12 and TGF-β polarization conditions. Data are expressed as fold change relative to the WT + IL-12 + TGF-β group. n = 6 independent experiments. Data are expressed as mean ± SD. $^{**}p < 0.01$; $^{***}p < 0.001$; $^{****}p < 0.0001$. For all panels, unpaired two-tailed Student's *t*-test was used for statistical analysis comparing WT and $PTPRO^{-/-}$ groups under the same culture conditions. IL-12, interleukin-12; TGF-β, transforming growth factor-β.

approximately 1.4 times the Treg percentage observed in WT cultures (Fig. 4B). This dramatic increase indicates that PTPRO deletion strongly favors Treg lineage commitment when TGF-β signals are present. Correspondingly, the Th1 subset was further suppressed in $PTPRO^{-/-}$ cultures. Only ~7% of $PTPRO^{-/-}$ $CD4^+$ cells were IFN-γ^+ (vs ~10% in WT, $p < 0.05$), and TNF-α^+ cells were also fewer (6% in $PTPRO^{-/-}$ vs ~15% in WT, Fig. 4B). These data re-

inforce that PTPRO deficiency intrinsically shifts $CD4^+$ T cells away from Th1 and toward Treg differentiation, even when both types of polarization signals are present.

Gene expression measurements further corroborated the flow cytometry results. RNA was extracted from the cultured T cells, and lineage-specific gene expression was analyzed by RT-qPCR. Under Th1-polarizing conditions (IL-12 without TGF-β), $PTPRO^{-/-}$ T cells showed significantly lower *IFN-*γ and *TNF-*α mRNA levels compared to WT cells (Fig. 4C). Under combined IL-12 + TGF-β conditions, the genotype differences became even more pronounced (Fig. 4D). $PTPRO^{-/-}$ T cells had markedly lower Th1 cytokine expression, with reduced *IFN-*γ and *TNF-*α mRNA levels compared to WT, and substantially higher *Foxp3* expression (>3-fold increase, $p < 0.05$, Fig. 4D). This robust upregulation of *Foxp3* in $PTPRO^{-/-}$ cells exposed to TGF-β reflects their heightened Treg differentiation capacity. Together, the mRNA data align with the immunophenotyping, confirming that loss of PTPRO intrinsically dampens the Th1 program and facilitates the generation of Tregs in $CD4^+$ T cells.

PTPRO Regulates Treg Differentiation via the JAK2-STAT5 Pathway

Our results so far indicate that PTPRO constrains Treg development. We next explored the molecular mechanism behind this effect, focusing on the JAK-STAT signaling axis. STAT5 is a transcription factor crucial for Treg differentiation; it is activated downstream of IL-2 and drives *Foxp3* expression when appropriately stimulated. We hypothesized that PTPRO might influence the Th1/Treg balance by modulating the phosphorylation status of JAK2 and STAT5. This hypothesis was informed by reports that PTPRO can dephosphorylate JAK family kinases, and specifically that PTPRO can negatively regulate JAK2 activation in other cell types. We first conducted co-immunoprecipitation (Co-IP) experiments with colon lysates to test whether PTPRO and JAK2 physically associate. Indeed, immunoprecipitating PTPRO from WT colon lysates pulled down JAK2 (detected by anti-JAK2 western blot; Fig. 5A). Conversely, immunoprecipitating JAK2 brought down PTPRO. These reciprocal Co-IPs confirm that PTPRO and JAK2 form a complex in colonic cells, suggesting that PTPRO can bind JAK2 and potentially modulate its phosphorylation state.

We next compared JAK2 and STAT5 activation in DSS-treated WT vs. $PTPRO^{-/-}$ mice. Colonic lysates from these mice were analyzed by western blotting for total and phosphorylated JAK2 and STAT5. As shown in Fig. 5B (quantified in the right panel), the absence of PTPRO led to hyperactivation of the JAK2-STAT5 pathway. $PTPRO^{-/-}$ colons had significantly higher levels of p-Jak2 (Tyr1007/Tyr1008) than WT colons (Fig. 5B). Densitometry indicated approximately a 4-fold increase in p-JAK2 in $PTPRO^{-/-}$ samples (normalized to total JAK2, $p < 0.05$, Fig. 5B). Similarly, p-STAT5 (Tyr694) was ~2-fold higher in $PTPRO^{-/-}$ colons compared to WT (Fig. 5B). Importantly, total JAK2 and total STAT5 levels were similar between WT and $PTPRO^{-/-}$, indicating that the differences were specific to phosphorylation (Fig. 5B). In other words, PTPRO deficiency resulted in excessive JAK2-STAT5 activation in the inflamed colon. This finding is consistent with the notion that PTPRO normally acts as a negative regulator of JAK2; in its absence, JAK2 remains hyper-phosphorylated (constitutively active), driving increased STAT5 activation. The heightened STAT5 activity in $PTPRO^{-/-}$ mice correlates with their increased Treg differentiation, since STAT5 signaling is a key promoter of $Foxp3^+$ Treg development.

To establish a causal relationship between PTPRO activity and JAK2-STAT5 signaling, we performed *in vitro* experiments by adding exogenous recombinant PTPRO protein to T cell cultures and examining the effect on pathway activation. Naive $CD4^+$ T cells were stimulated under Treg-polarizing conditions (TGF-β + anti-CD3/CD28) and treated with increasing concentrations of recombinant PTPRO (0, 25, 50, or 100 µg/mL). After 24 h, cells were analyzed by western blotting for p-JAK2 and p-STAT5. The results (Fig. 5C) showed that PTPRO caused a dose-dependent suppression of JAK2 and STAT5 phosphorylation. At the highest dose (100 µg/mL), p-JAK2 and p-STAT5 levels were dramatically reduced (Fig. 5C). Quantification confirmed a significant reduction in p-JAK2 and p-STAT5 at 50 and 100 µg/mL PTPRO (both $p < 0.05$ vs. 0 µg/mL, Fig. 5C). These data indicate that exogenous PTPRO enzymatic activity can directly dephosphorylate and inactivate JAK2-STAT5 signaling in T cells.

To validate these findings at the single-cell level, we performed intracellular phospho-flow cytometry for p-JAK2 and p-STAT5 under the same conditions. As the dose of PTPRO increased, the percentage of p-$JAK2^+$ cells declined substantially (Fig. 5D). At 100 µg/mL PTPRO, fewer than 30% of cells were p-$JAK2^+$, indicating effective JAK2 dephosphorylation in the majority of cells (Fig. 5D). A similar dose-dependent decline was observed in p-STAT5 levels (Fig. 5E). These phospho-flow results corroborate the western blots, reinforcing that PTPRO directly attenuates JAK2-STAT5 activation in $CD4^+$ T cells. Taken together, the *in vivo* and *in vitro* evidence strongly implicates the JAK2-STAT5 pathway as a primary target of PTPRO's phosphatase activity in the immune system.

To further confirm that enhanced JAK2-STAT5 signaling underlies the protective phenotype in $PTPRO^{-/-}$ mice, we administered the selective JAK2 inhibitor AZD1480 to DSS-treated mice. Flow cytometry of colonic lymphocytes revealed that JAK2 inhibition largely eliminated the Th1/Treg differences between $PTPRO^{-/-}$ and WT mice (Fig. 5F). As expected, vehicle-treated $PTPRO^{-/-}$ mice showed the characteristic low-Th1/high-Treg profile (fewer IFN-γ^+ $CD4^+$ cells and more $Foxp3^+$ $CD4^+$ cells)

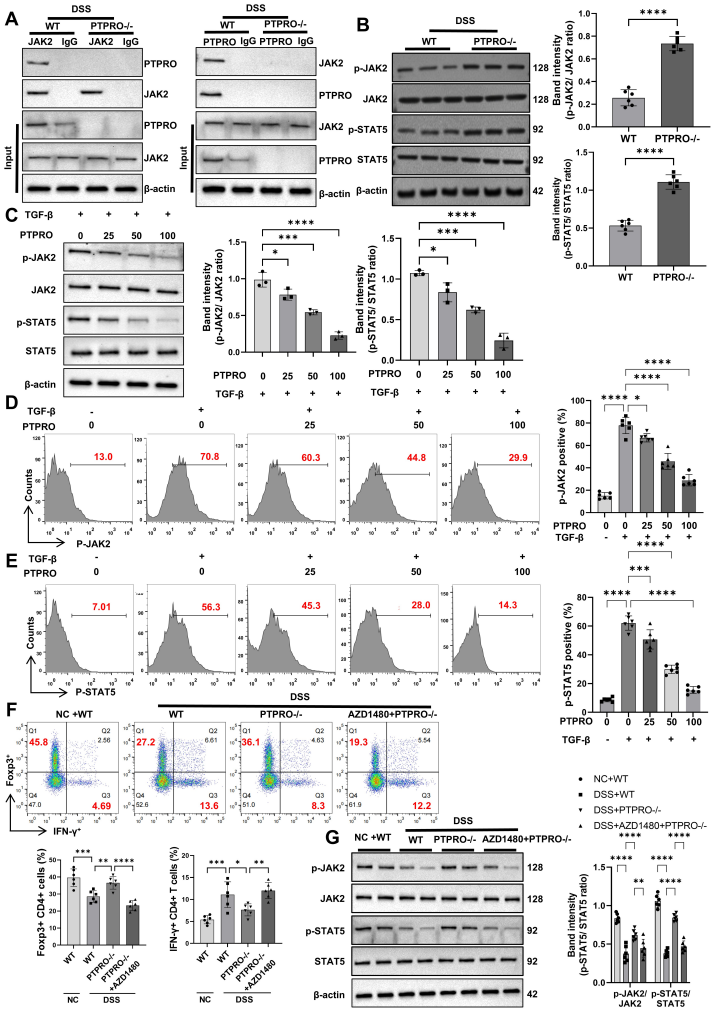

Fig. 5. PTPRO inhibition promotes Treg differentiation through the JAK2-STAT5 signaling pathway. (A) Co-immunoprecipitation experiment in mouse colon tissues showing that PTPRO can bind to JAK2. (B) Western blot analysis of JAK2-STAT5 signaling pathway proteins in colon tissues from WT and PTPRO$^{-/-}$ mice under DSS treatment. Representative blots (left) and densitometric quantification (right) showing p-JAK2, JAK2, p-STAT5, STAT5, and β-actin expression levels. Protein levels were normalized to their respective total proteins or β-actin. n = 6 mice per group. (C) Dose-dependent effects of recombinant PTPRO protein on JAK2-STAT5 signaling in TGF-β-stimulated native CD4$^+$ T cells. Cells were treated with increasing concentrations of PTPRO protein (0, 25, 50, 100 µg/mL) for 24 h. Representative western blots (left) and densitometric quantification (right) showing p-JAK2, JAK2, p-STAT5, STAT5, and β-actin expression levels. n = 3–6 independent experiments. (D) Flow cytometry analysis of p-JAK2 expression in TGF-β-stimulated CD4$^+$ T cells treated with different concentrations of recombinant PTPRO protein. Representative histograms (left) showing p-JAK2 mean fluorescence intensity (MFI) with quantitative analysis (right). Red numbers indicate the percentage of p-JAK2$^+$ cells. n = 6 independent experiments. (E) Flow cytometry analysis of p-STAT5 expression in TGF-β-stimulated CD4$^+$ T cells treated with different concentrations of recombinant PTPRO protein. Representative histograms (left) showing p-STAT5 MFI with quantitative analysis (right). Red numbers indicate percentage of p-STAT5$^+$ cells. n = 6 independent experiments. (F) Flow cytometry analysis of IFN-γ^+ CD4$^+$ T cells (Th1) and Foxp3$^+$ CD4$^+$ T cells (Treg) in colon lamina propria from DSS-treated mice with or without JAK2 inhibitor AZD1480 treatment. Representative flow cytometry plots (upper) and quantitative analysis (lower). Mice received daily intraperitoneal injections of AZD1480 (30 mg/kg) or vehicle control starting from day 0. Red numbers indicate percentages of positive cells within the CD4$^+$ gate. n = 6 mice per group. (G) Western blot analysis of p-JAK2 and p-STAT5 proteins in colon tissues from DSS-treated mice with or without JAK2 inhibitor AZD1480 treatment. Representative western blots (left) and densitometric quantification (right) showing p-JAK2, JAK2, p-STAT5, STAT5, and β-actin expression levels. n = 6 mice per group. Data are expressed as mean ± SD. *$p < 0.05$; **$p < 0.01$; ***$p < 0.001$; ****$p < 0.0001$. For (B), unpaired two-tailed Student's t-test was used; for (C), (D), (E), and (F), one-way ANOVA followed by Tukey post-hoc test was performed. JAK2, Janus kinase 2; p-JAK2, phosphorylated JAK2; STAT5, signal transducer and activator of transcription 5; p-STAT5, phosphorylated STAT5; IgG, immunoglobulin G.

(Fig. 5F). However, Th1 cell frequency increased to near WT levels and Treg frequency significantly decreased in PTPRO$^{-/-}$ mice treated with AZD1480 (Fig. 5F, lower panel). We also confirmed that AZD1480 treatment effectively reduced p-STAT5 levels in PTPRO$^{-/-}$ T cells (Fig. 5G), consistent with the inhibition of the JAK2-STAT5 pathway. These results indicate that the expansion of Tregs and suppression of Th1 cells in PTPRO$^{-/-}$ mice depends on intact JAK2-STAT5 signaling.

JAK2 Inhibition Abrogates the Protective Effect of PTPRO Deficiency in Colitis

If the protective effect of PTPRO deficiency in colitis is mediated by enhanced JAK2-STAT5 signaling (and the resulting increase in Tregs), then pharmacologically blocking JAK2 should abolish that benefit. We tested this hypothesis by administering the JAK2 inhibitor AZD1480 to PTPRO$^{-/-}$ mice during DSS colitis (Fig. 6A). PTPRO$^{-/-}$ mice normally lost minimal weight under DSS, but with AZD1480 they underwent rapid, severe weight loss akin to WT mice (Fig. 6B). Accordingly, the DAI of AZD1480-treated PTPRO$^{-/-}$ mice rose dramatically (Fig. 6C). By day 12, these mice reached DAI scores of ~7–8, compared to only ~4–5 in PTPRO$^{-/-}$ mice on vehicle (Fig. 6C). In fact, PTPRO$^{-/-}$ mice given AZD1480 were statistically indistinguishable from WT mice in DAI, demonstrating that JAK2 inhibition largely abolished the disease resistance of PTPRO deficiency (Fig. 6C).

Macroscopic and histological analyses corroborated these findings. DSS exposure shortened WT colons to ~5.2 cm, whereas PTPRO$^{-/-}$ colons remained ~6.7 cm on vehicle. However, PTPRO$^{-/-}$ colons on AZD1480 were severely shortened (~5.6 cm), on par with WT (Fig. 6D). These inhibitor-treated PTPRO$^{-/-}$ colons were as swollen, hyperemic, and contracted as those of WT mice, indicating substantial inflammation. Histologically, PTPRO$^{-/-}$ colons treated with AZD1480 showed extensive damage similar to WT colitis (Fig. 6E). While PTPRO$^{-/-}$ colons on vehicle had only mild, superficial inflammation (Fig. 6E), those receiving AZD1480 exhibited largely denuded mucosa with deep ulcerations and dense inflammatory infiltrates penetrating the submucosa (Fig. 6E). The histology score for PTPRO$^{-/-}$ mice surged with JAK2 inhibition, reaching ~9–10 (vs ~7 with vehicle, $p < 0.05$, Fig. 6F). Again, PTPRO$^{-/-}$ + AZD1480 mice were comparable to WT mice in histology score (Fig. 6F).

Moreover, we measured representative Th1 and Treg markers in colonic tissues across groups to determine whether the immune signature of PTPRO$^{-/-}$ was reversed by JAK2 inhibition. By RT-qPCR, vehicle-treated PTPRO$^{-/-}$ colons had much lower *IFN-γ* and higher *Foxp3* compared to WT (Fig. 6G,H). Upon JAK2 inhibition, the *IFN-γ* mRNA level in PTPRO$^{-/-}$ + AZD1480 mice was elevated comparable to PTPRO$^{-/-}$ mice (Fig. 6G). Conversely, *Foxp3* mRNA in PTPRO$^{-/-}$ + AZD1480 mice plummeted to ~30% of the level in untreated PTPRO$^{-/-}$ mice ($p < 0.05$), essentially negating the *Foxp3* elevation that PTPRO deficiency normally confers (Fig. 6H). Finally, we evaluated goblet cell preservation using AB/PAS staining. As noted, vehicle-treated PTPRO$^{-/-}$ mice retained abundant goblet cells despite DSS (Fig. 6I). However, PTPRO$^{-/-}$ mice on AZD1480 lost this goblet cell protection (Fig. 6I). Their goblet cell counts dropped to ~120 cells per field, equivalent to the severe depletion in WT DSS mice (Fig. 6I). This indicates that maintenance of the mucus barrier in PTPRO$^{-/-}$ colitis also depended on JAK2-STAT5 activity (likely via IL-10 and Treg-associated repair factors), and when that pathway was blocked, mucosal damage proceeded unchecked.

Discussion

In this study, we have identified PTPRO as a key regulator of intestinal inflammation and immune homeostasis in ulcerative colitis. We demonstrated that PTPRO expression is significantly elevated in active UC, and that PTPRO deficiency dramatically reduces colitis severity by shifting CD4$^+$ T cell responses away from pathogenic Th1 immunity and toward protective Treg activity. Mechanistically, our data indicate that PTPRO mediates these effects via the JAK2-STAT5 signaling pathway: PTPRO normally acts as a negative regulator of STAT5 phosphorylation, thereby constraining Treg differentiation. When PTPRO is absent, JAK2/STAT5 signaling is hyperactive, promoting Foxp3$^+$ Treg development and tempering inflammation. Conversely, blocking JAK2 signaling in PTPRO$^{-/-}$ mice negated the benefits of PTPRO loss, confirming that PTPRO's pro-inflammatory influence in colitis operates through this pathway. Collectively, our findings shed new light on how dysregulated tyrosine phosphatase activity can contribute to Th1/Treg imbalance in UC, and they suggest that PTPRO may represent a novel therapeutic target for rebalancing the immune response in this disease.

Our study establishes a clear correlation between PTPRO expression and UC disease activity. We observed that *PTPRO* mRNA and protein were significantly upregulated in the colonic tissues of both DSS-treated colitic mice and UC patients, especially those with more severe disease. This finding is consistent with prior studies linking PTPRO to inflammatory conditions. Previous studies have shown that PTPRO levels are elevated in UC patients with active disease and correlate with endoscopic severity [21]. Similarly, increased PTPRO expression has been documented in a variety of chronic inflammatory diseases, often associated with worse clinical outcomes. For example, in the context of inflammation related to obesity [18], the truncated isoform PTPROt exacerbates liver inflammation in NASH. By adding UC to the list of conditions with PTPRO overexpression, our data suggest that PTPRO could serve as a biomarker of intestinal inflammatory activity. Clinically,

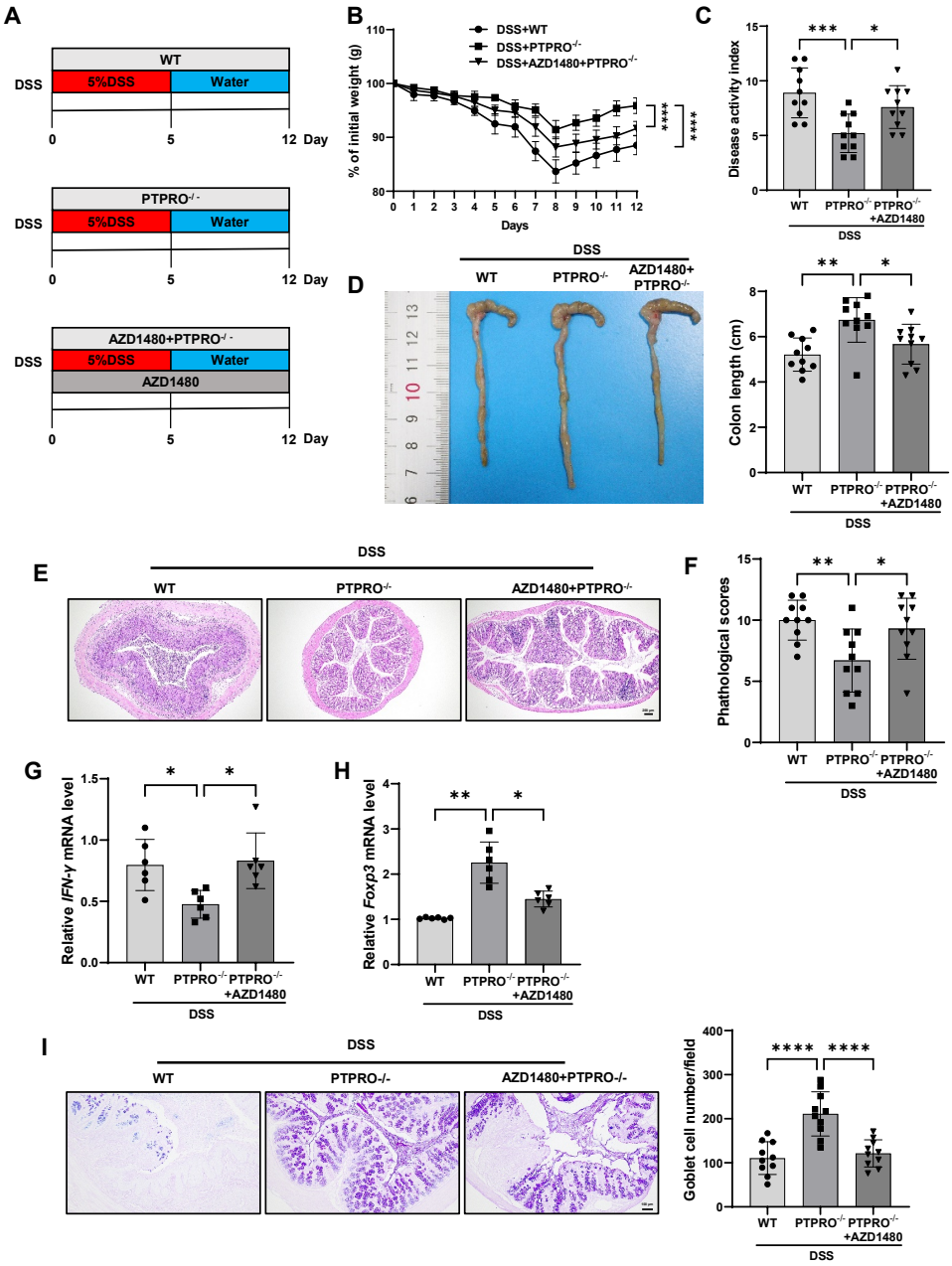

Fig. 6. JAK2 inhibition blocks the protective effect of PTPRO knockout on ulcerative colitis in mice. (A) Experimental design schematic for panels (B–I). WT and PTPRO$^{-/-}$ mice were treated with DSS and received daily intraperitoneal injections of either vehicle control or JAK2 inhibitor AZD1480 (30 mg/kg) starting from day 0. Mice received drinking water containing 5% (w/v) DSS from day 0 to day 5, followed by normal water for 7 days. (B) Body weight changes during the experimental period. Data are expressed as percentage of initial body weight. n = 10 mice per group. (C) DAI scores measured on day 12. DAI was calculated as the sum of weight loss, stool consistency, and rectal bleeding scores. n = 10 mice per group. (D) Representative images of colon tissues from each experimental group and quantification of colon length. Scale bar represents 1 cm. n = 10 mice per group. (E) Representative H&E staining images of distal colon from each experimental group showing histopathological changes. Scale bar, 200 μm. (F) Histopathological scores evaluating inflammation severity, tissue damage, and architectural distortion. n = 10 mice per group. (G,H) Detection of *IFN-γ* (G) and *Foxp3* (H) mRNA expression levels in mouse colon tissues by RT-qPCR. Data are expressed as fold change relative to the DSS + WT group. n = 6 mice per group. (I) Representative AB/PAS staining images showing goblet cells (purple-stained) in colon crypts from each experimental group (left) and quantification of goblet cell numbers per field (right). At least 20 well-oriented crypts were counted per mouse. Scale bar, 100 μm. n = 10 mice per group. Data are expressed as mean ± SD. *$p < 0.05$; **$p < 0.01$; ***$p < 0.001$; ****$p < 0.0001$. For (B), two-way ANOVA with repeated measures followed by Bonferroni post-hoc test was performed; for (C), (D), (F), (G), (H), and (I), one-way ANOVA followed by Tukey post-hoc test was used for statistical analysis.

if high PTPRO levels in biopsy tissue reflect UC severity (as our patient data suggest), monitoring PTPRO expression might help in evaluating disease progression or predicting flares.

Functionally, we showed that genetic ablation of PTPRO provides significant protection against colitis. PTPRO$^{-/-}$ mice had markedly less weight loss, lower DAI scores, and improved histopathology compared to WT mice after DSS exposure. The knockout mice had minimal ulceration and preserved crypt architecture, indicating that the tissue damage normally caused by DSS was greatly reduced. This observation suggests that PTPRO actively drives inflammatory injury. Consistent with this, PTPRO$^{-/-}$ mice maintained near-normal goblet cell numbers and mucin levels, suggesting an intact epithelial barrier despite the inflammatory insult. Moreover, PTPRO$^{-/-}$ colons displayed a cytokine profile skewed toward anti-inflammatory mediators (low IFN-γ, TNF-α, IL-6, and IL-1β, and high IL-10), a profile known to favor resolution of inflammation and tissue healing. This phenotype closely resembles other contexts in which pathogenic T cell responses are curbed. For instance, mice deficient in certain Th1/Th17-driving factors or mice treated with Treg-boosting therapies often show milder colitis and preserved mucus layers. Thus, our results indicate that PTPRO is a critical endogenous promoter of colitis pathogenesis, likely sustaining pro-inflammatory immune pathways that lead to tissue damage. Removing PTPRO (genetically or potentially pharmacologically) effectively "rebalances" the immune response and protects the intestinal mucosa.

A central discovery of this work is that PTPRO deletion restores the balance of CD4$^+$ T cell subsets in favor of Tregs over Th1 cells. An imbalance between Th1 and Treg cells is a hallmark of IBD immunopathology: excessive Th1 (and Th17) responses coupled with inadequate Treg suppression contribute to chronic inflammation [27]. In our DSS colitis model, PTPRO$^{-/-}$ mice showed a dramatic correction of this imbalance: they had significantly fewer colonic Th1 cells and approximately double the Treg frequency of WT mice. This *in vivo* rebalancing was mirrored by our *in vitro* experiments, which showed that PTPRO-deficient T cells are intrinsically less prone to differentiate into IFN-γ^+ Th1 cells and more inclined to become Foxp3$^+$ Tregs. Notably, even under strongly Th1-polarizing conditions, PTPRO$^{-/-}$ T cells exhibited an increased tendency to express Foxp3, and under Treg-favoring conditions, they generated Tregs at much higher rates than WT cells. These observations suggest that PTPRO normally acts within T cells to favor inflammatory (Th1) differentiation while restraining the induction of regulatory phenotypes. Our findings are consistent with earlier evidence that PTPRO influences T cell behavior. For example, PTPROt (the immune isoform of PTPRO) helps sustain T cell activation in the tumor microenvironment of liver cancer. Moreover, recent research has associated high PTPRO expression with enhanced Th1 and cytotoxic T cell infiltration in certain diseases [28]. We extend these insights to IBD by showing that PTPRO is a novel modulator of mucosal T cell responses whose absence promotes immune tolerance. In essence, PTPRO functions as a pro-inflammatory "switch" that tilts the balance toward Th1-driven immunity at the expense of Treg-mediated regulation. When this switch is turned off (as in PTPRO$^{-/-}$ mice), the immune system defaults to a more regulated state that better controls inflammation. This makes PTPRO an attractive target for therapy, since modulating it could help restore the disturbed Th1/Treg equilibrium in UC patients.

Our mechanistic studies identified the JAK2-STAT5 pathway as a major downstream target of PTPRO in T cells. We found that PTPRO interacts with JAK2, a pivotal kinase in multiple cytokine signaling pathways. However, we did not investigate whether the interaction between PTPRO and JAK2 is direct or indirect via other proteins. This represents a limitation of our study that merits further investigation in future research. Under normal conditions, PTPRO likely dephosphorylates JAK2 to keep its activity in check [29]. In the absence of PTPRO, JAK2 becomes hyperactivated, leading to excessive STAT5 phosphorylation. STAT5 is well known to drive *Foxp3* expression and stabilize Treg differentiation in the presence of TGF-β [30,31]. Therefore, the enhanced STAT5 activation in PTPRO$^{-/-}$ T cells offers a plausible explanation for their Treg expansion. In our experiments, PTPRO$^{-/-}$ mice exhibited elevated colonic STAT5 phosphorylation along with increased Foxp3$^+$ Tregs, whereas WT mice had lower STAT5 activity and fewer Tregs. We established causality for this mechanism in two ways: by reintroducing PTPRO protein and by inhibiting JAK2. Adding recombinant PTPRO protein to T cell cultures caused a dose-dependent suppression of JAK2 and STAT5 phosphorylation, confirming that PTPRO can dampen JAK2-STAT5 signaling. Conversely, pharmacological JAK2 inhibition in PTPRO$^{-/-}$ mice abolished the STAT5 signal sustaining their Tregs, causing the Treg population to decline and Th1-mediated inflammation to rebound. Essentially, blocking JAK2 made PTPRO$^{-/-}$ mice resemble PTPRO-sufficient mice in terms of T cell balance and colitis severity. These findings underscore that PTPRO's impact on the Th1/Treg balance is executed through its control of JAK2-STAT5 signaling. It is worth noting that JAK2 transmits signals for many cytokines (IL-6, IL-12, IL-23, and granulocyte–macrophage colony-stimulating factor, among others), so PTPRO might influence multiple arms of the immune response. However, STAT5 activation is most critically tied to IL-2 family cytokines that promote Treg survival and expansion. Our data suggest that the PTPRO-JAK2 interaction predominantly affects the JAK2/STAT5 axis in CD4$^+$ T cells, thereby altering Treg outcomes.

The importance of JAK-STAT pathways in IBD pathogenesis and therapy is well established [32]. Abnormal ac-

tivation of various JAK/STAT members has been observed in IBD, and broad-spectrum JAK inhibitors like tofacitinib (which targets JAK1/3) are effective in treating moderate-to-severe UC by suppressing inflammatory cytokine signaling [33]. Our findings add nuance to this paradigm by showing that specific modulation of the JAK2-STAT5 axis in certain immune cells can yield therapeutic benefits by enhancing regulatory immunity. Conventional JAK inhibition in IBD works by broadly dampening effector lymphocytes and inflammatory cytokines—effective for inflammation control, but potentially compromising some host defenses. In contrast, PTPRO deficiency represents a more targeted form of immune modulation. It selectively amplifies JAK2/STAT5 signaling in T cells, resulting in Treg expansion and suppression of inflammation without globally disabling the immune system. Interestingly, a recent study in an autoimmune encephalomyelitis model found that partial inhibition of JAK2/STAT5 skewed T cells away from pathogenic phenotypes [34]. In our colitis model, however, inhibition of JAK2 eliminated Tregs and worsened disease. These observations suggest that the timing, context, and degree of JAK-STAT modulation can have very different outcomes—there is a fine balance between controlling pathogenic inflammation and maintaining immune regulation. Our work suggests that inhibiting a negative regulator like PTPRO might achieve a therapeutic immune rebalance (enhancing Treg function) that is distinct from, yet complementary to, the effects of direct JAK inhibition. In other words, rather than only blocking inflammatory signals, therapy could also aim to harness the body's own regulatory mechanisms.

Our study points to PTPRO as a potential therapeutic target in UC. If small-molecule inhibitors or antagonists of PTPRO can be developed (or repurposed from other indications), they could pharmacologically mimic the PTPRO-deficient condition. By inhibiting PTPRO in intestinal immune cells, one would expect enhanced STAT5 activation and Treg responses, thereby quelling inflammation. A parallel can be drawn to PTPN22, another phosphatase for which inhibitors have been explored to boost Treg function in autoimmune models. However, it is important to acknowledge that targeting phosphatases is challenging and requires high specificity to avoid off-target effects. PTPRO is expressed in multiple tissues (most notably kidney podocytes, where it was first characterized), so systemic PTPRO inhibition could carry risks such as kidney dysfunction (e.g., proteinuria) [35]. Therefore, any therapeutic strategy would need to minimize off-target exposure—possible approaches include colon-targeted drug delivery or developing biologics that block PTPRO specifically in gut immune cells. Alternatively, there is growing interest in treatments that enhance regulatory immunity (for instance, low-dose IL-2 therapy to expand Tregs in autoimmune diseases) [36,37]. A PTPRO inhibitor could be combined with such treatments. Conceptually, PTPRO inhibition might achieve a similar effect by relieving the JAK2-STAT5 axis from negative regulation, thereby amplifying IL-2 signaling and promoting Treg proliferation. However, any such approach must be finely tuned—excessive STAT5 activation can have unwanted consequences (e.g., potentially promoting aberrant cell growth or affecting other cell types). Thus, a PTPRO-targeted therapy would require careful calibration. Nonetheless, our results provide proof-of-principle that modulating a phosphatase can tilt the immune response toward resolution of inflammation without broadly immunosuppressing the host.

While our study provides significant insights, it also raises questions for future investigation. First, the DSS model we used primarily reflects innate immune–driven colitis. Although we observed T cell changes, this model might not capture all aspects of human UC immunopathology. It will be valuable to examine PTPRO's role in other IBD models, such as T cell transfer colitis or chronic chemically induced colitis, to determine the generalization of our findings. Second, our patient data show a correlation between PTPRO levels and disease severity, but the causation is not established. It remains to be determined whether high PTPRO in patients is merely a marker of inflammation or actively contributes to it. Tracking PTPRO expression longitudinally in patients receiving treatment (to determine whether it decreases with successful therapy) could clarify its role as a biomarker or mediator. Third, at the cellular level, the specific immune cell types in which PTPRO acts to promote colitis are not fully defined. We have strong evidence for a T cell–intrinsic role, but PTPRO is also expressed in macrophages, B cells, and other immune cells [38]. In prior studies, researchers found that PTPRO and the TLR4/NF-κB signaling pathway were upregulated in damaged intestinal mucosa and lamina propria mononuclear cells of ulcerative colitis patients [21]. This study also revealed that PTPRO-overexpressing macrophages enhance NF-κB/p65 phosphorylation, thereby inhibiting intestinal epithelial cell proliferation and promoting apoptosis [21]. Moreover, tumor-derived exosomal PTPRO induces M1-like macrophage polarization and suppresses STAT signaling, thus inhibiting breast cancer progression [39]. Wang *et al*. [40] demonstrated that PTPRO downregulation promotes M2 macrophage polarization in gestational diabetes. Given that TLR4/NF-κB signaling regulation is closely linked to the balance of M1/M2 macrophage polarization, PTPRO's effect on macrophage polarization (M1 vs. M2) could also influence colitis outcomes, as macrophages are key players in mucosal innate immunity [38]. It would be interesting to investigate whether PTPRO$^{-/-}$ mice have altered macrophage or dendritic cell functions. Future studies using cell type–specific PTPRO knockouts (e.g., T cell–specific or myeloid-specific deletion) could dissect the contributions of different compartments. Additionally, our finding that PTPRO binds JAK2 prompts questions about which upstream signals regulate PTPRO during colitis. Al-

though we observed that PTPRO is induced by DSS and in active UC, the triggers for this upregulation warrant further investigation.

Conclusion

In conclusion, we have identified PTPRO as a novel player in the immunopathology of ulcerative colitis. PTPRO aggravates colitis by promoting Th1-mediated inflammation and inhibiting Treg differentiation through suppression of JAK2-STAT5 signaling. Conversely, in the absence of PTPRO, enhanced STAT5 activation leads to increased Treg responses and amelioration of intestinal inflammation. These findings not only illuminate fundamental mechanisms governing T cell balance in the gut but also highlight PTPRO as a potential therapeutic target. By targeting PTPRO or its downstream effects, it may be possible to restore immune tolerance in UC and relieve chronic inflammation. Future research should explore the therapeutic potential of PTPRO, including developing PTPRO inhibitors or related strategies and testing their safety and efficacy in preclinical models. Additionally, investigating PTPRO's role across different phases of IBD (disease initiation, flare, and remission) and its interactions with other pathways (such as NF-κB, STAT3, or metabolic checkpoints) will deepen our understanding of how this phosphatase orchestrates immune cell function. In summary, our work provides a strong rationale for further exploration of PTPRO in IBD pathogenesis and therapy, potentially paving the way for more targeted immunomodulatory treatments for UC and related inflammatory disorders.

Availability of Data and Materials

The data that support the findings of this study are available from the corresponding authors upon reasonable request.

Author Contributions

XZ, LX and MW designed the research study. XZ, XC and RH performed the research. LJ, JL, WT and CY contributed to data collection and experimental procedures. XZ and XC analyzed the data. XZ, XC and RH wrote the manuscript. All authors contributed to important editorial changes in the manuscript. All authors read and approved the final manuscript. All authors have participated sufficiently in the work and agreed to be accountable for all aspects of the work.

Ethics Approval and Consent to Participate

All animal experimental procedures were conducted in strict accordance with institutional and national guidelines for the care and use of laboratory animals, and received prior approval from the Institutional Animal Ethics Committee (Approval No. IEC2023051201). The use of human pathological specimens in this study was approved by the Ethics Committee of the Affiliated Wuxi People's Hospital of Nanjing Medical University (Approval No. KY23087) and was conducted in full compliance with the principles outlined in the Declaration of Helsinki.

Acknowledgment

Not applicable.

Funding

This work was supported by Wuxi Municipal Health Commission project (No. T202320), Soft Project of Wuxi Science and Technology Association (No. KX-23-C038), and The Young and Middle-Aged Talents Program of Wuxi Health Commission (BJ2020011).

Conflict of Interest

The authors declare no conflict of interest.

Supplementary Material

Supplementary material associated with this article can be found, in the online version, at https://doi.org/10.24976/Discov.Med.202537202.231.

References

[1] Chang YL, Lo HY, Cheng SP, Chang KT, Lin XF, Lee SP, *et al*. Therapeutic effects of a single injection of human umbilical mesenchymal stem cells on acute and chronic colitis in mice. Scientific Reports. 2019; 9: 5832. https://doi.org/10.1038/s41598-019-41910-x.

[2] Min X, Guo Y, Zhou Y, Chen X. Protection against Dextran Sulfate Sodium-Induced Ulcerative Colitis in Mice by Neferine, A Natural Product from *Nelumbo nucifera Gaertn*. Cell Journal. 2021; 22: 523–531. https://doi.org/10.22074/cellj.2021.6918.

[3] Tang X, Huang Y, Zhu Y, Xu Y. Immune dysregulation in ulcerative colitis: pathogenic mechanisms and therapeutic strategies of traditional Chinese medicine. Frontiers in Cell and Developmental Biology. 2025; 13: 1610435. https://doi.org/10.3389/fcell.2025.1610435.

[4] Wang Y, Tian J, Tang X, Rui K, Tian X, Ma J, *et al*. Exosomes released by granulocytic myeloid-derived suppressor cells attenuate DSS-induced colitis in mice. Oncotarget. 2016; 7: 15356–15368. https://doi.org/10.18632/oncotarget.7324.

[5] Zhang S, Luo H, Sun S, Zhang Y, Ma J, Lin Y, *et al*. *Salvia miltiorrhiza* Bge. (Danshen) for Inflammatory Bowel Disease: Clinical Evidence and Network Pharmacology-Based Strategy for Developing Supplementary Medical Application. Frontiers in Pharmacology. 2022; 12: 741871. https://doi.org/10.3389/fphar.2021.741871.

[6] Wang S, Su W, Wu X, Dong W. Restoring Treg/Th17 cell balance in ulcerative colitis through HRas silencing and MAPK pathway inhibition. International Immunopharmacology. 2024; 130: 111608. https://doi.org/10.1016/j.intimp.2024.111608.

[7] Lv L, Chen Z, Bai W, Hao J, Heng Z, Meng C, *et al*. Tauro-hyodeoxycholic acid alleviates trinitrobenzene sulfonic acid in-

duced ulcerative colitis via regulating Th1/Th2 and Th17/Treg cells balance. Life Sciences. 2023; 318: 121501. https://doi.org/10.1016/j.lfs.2023.121501.

[8] Sun X, Huang X, Sun X, Chen S, Zhang Z, Yu Y, *et al*. Oxidative Stress-Related lncRNAs Are Potential Biomarkers for Predicting Prognosis and Immune Responses in Patients With LUAD. Frontiers in Genetics. 2022; 13: 909797. https://doi.org/10.3389/fgene.2022.909797.

[9] Wang S, Dong H, Han J, Ho WT, Fu X, Zhao ZJ. Identification of a variant form of tyrosine phosphatase LYP. BMC Molecular Biology. 2010; 11: 78. https://doi.org/10.1186/1471-2199-11-78.

[10] Kim WK, Jung H, Kim EY, Kim DH, Cho YS, Park BC, *et al*. RPTPμ tyrosine phosphatase promotes adipogenic differentiation via modulation of p120 catenin phosphorylation. Molecular Biology of the Cell. 2011; 22: 4883–4891. https://doi.org/10.1091/mbc.E11-03-0175.

[11] Xu J, Zeng LF, Shen W, Turchi JJ, Zhang ZY. Targeting SHP2 for EGFR inhibitor resistant non-small cell lung carcinoma. Biochemical and Biophysical Research Communications. 2013; 439: 586–590. https://doi.org/10.1016/j.bbrc.2013.09.028.

[12] Verstrepen L, Beyaert R. Receptor proximal kinases in NF-κB signaling as potential therapeutic targets in cancer and inflammation. Biochemical Pharmacology. 2014; 92: 519–529. https://doi.org/10.1016/j.bcp.2014.10.017.

[13] Li SY, Li R, Chen YL, Xiong LK, Wang HL, Rong L, *et al*. Aberrant PTPRO methylation in tumor tissues as a potential biomarker that predicts clinical outcomes in breast cancer patients. BMC Genetics. 2014; 15: 67. https://doi.org/10.1186/1471-2156-15-67.

[14] Wang A, Zhang Y, Lv X, Liang G. Therapeutic potential of targeting protein tyrosine phosphatases in liver diseases. Acta Pharmaceutica Sinica. B. 2024; 14: 3295–3311. https://doi.org/10.1016/j.apsb.2024.05.006.

[15] Huan Z, Tang Y, Xu C, Cai J, Yao H, Wang Y, *et al*. PTPRO knockdown protects against inflammation in hemorrhage shock-induced lung injury involving the NF-κB signaling pathway. Respiratory Research. 2022; 23: 195. https://doi.org/10.1186/s12931-022-02118-2.

[16] Hao M, Guo M, Yan R. Protein tyrosine phosphatase receptor-type O expression as a prognostic marker in patients with acute coronary syndrome undergoing percutaneous coronary intervention: A prospective study. Experimental and Therapeutic Medicine. 2021; 21: 435. https://doi.org/10.3892/etm.2021.9852.

[17] Hou X, Du J, Fang H. PTPRO is a therapeutic target and correlated with immune infiltrates in pancreatic cancer. Journal of Cancer. 2021; 12: 7445–7453. https://doi.org/10.7150/jca.64661.

[18] Shintani T, Suzuki R, Takeuchi Y, Shirasawa T, Noda M. Deletion or inhibition of PTPRO prevents ectopic fat accumulation and induces healthy obesity with markedly reduced systemic inflammation. Life Sciences. 2023; 313: 121292. https://doi.org/10.1016/j.lfs.2022.121292.

[19] Jin K, Liu Y, Shi Y, Zhang H, Sun Y, Zhangyuan G, *et al*. PTPROt aggravates inflammation by enhancing NF-κB activation in liver macrophages during nonalcoholic steatohepatitis. Theranostics. 2020; 10: 5290–5304. https://doi.org/10.7150/thno.42658.

[20] Hou J, Deng L, Zhuo H, Lin Z, Chen Y, Jiang R, *et al*. PTPROt maintains T cell immunity in the microenvironment of hepatocellular carcinoma. Journal of Molecular Cell Biology. 2015; 7: 338–350. https://doi.org/10.1093/jmcb/mjv047.

[21] Zhao J, Yan S, Zhu X, Bai W, Li J, Liang C. PTPRO exaggerates inflammation in ulcerative colitis through TLR4/NF-κB pathway. Journal of Cellular Biochemistry. 2020; 121: 1061–1071. https://doi.org/10.1002/jcb.29343.

[22] Lin Z, Zhang J, Liu B, Hong Z, Chen Z, Huang X. Comprehensively Analyze the Prognosis Significance and Immune Implication of PTPRO in Lung Adenocarcinoma. Mediators of Inflammation. 2023; 2023: 5248897. https://doi.org/10.1155/2023/5248897.

[23] Dai Y, Shi S, Liu H, Zhou H, Ding W, Liu C, *et al*. Protein tyrosine phosphatase PTPRO represses lung adenocarcinoma progression by inducing mitochondria-dependent apoptosis and restraining tumor metastasis. Cell Death & Disease. 2024; 15: 11. https://doi.org/10.1038/s41419-023-06375-x.

[24] Zhang S, Nie Q, Sun Y, Zuo S, Chen C, Li S, *et al*. Bacteroides uniformis degrades β-glucan to promote Lactobacillus johnsonii improving indole-3-lactic acid levels in alleviating colitis. Microbiome. 2024; 12: 177. https://doi.org/10.1186/s40168-024-01896-9.

[25] Wirtz S, Popp V, Kindermann M, Gerlach K, Weigmann B, Fichtner-Feigl S, *et al*. Chemically induced mouse models of acute and chronic intestinal inflammation. Nature Protocols. 2017; 12: 1295–1309. https://doi.org/10.1038/nprot.2017.044.

[26] Jia L, Jiang Y, Wu L, Fu J, Du J, Luo Z, *et al*. Porphyromonas gingivalis aggravates colitis via a gut microbiota-linoleic acid metabolism-Th17/Treg cell balance axis. Nature Communications. 2024; 15: 1617. https://doi.org/10.1038/s41467-024-45473-y.

[27] Deng P, Li X, Wei Y, Liu J, Chen M, Xu Y, *et al*. The herbal decoction modified Danggui Buxue Tang attenuates immune-mediated bone marrow failure by regulating the differentiation of T lymphocytes in an immune-induced aplastic anemia mouse model. PloS One. 2017; 12: e0180417. https://doi.org/10.1371/journal.pone.0180417.

[28] Dong H, Xie C, Yao Z, Zhao R, Lin Y, Luo Y, *et al*. PTPRO-related CD8$^+$ T-cell signatures predict prognosis and immunotherapy response in patients with breast cancer. Frontiers in Immunology. 2022; 13: 947841. https://doi.org/10.3389/fimmu.2022.947841.

[29] Xiong X, Liu J, Wu X, Yao Z, Meng Y, Liu S, *et al*. PTPRO represses breast cancer lung metastasis by inhibiting the JAK2-YAP axis. Scientific Reports. 2025; 15: 7065. https://doi.org/10.1038/s41598-025-91341-0.

[30] Elmore JP, McGee MC, Nidetz NF, Anannya O, Huang W, August A. Tuning T helper cell differentiation by ITK. Biochemical Society Transactions. 2020; 48: 179–185. https://doi.org/10.1042/BST20190486.

[31] Lourenço JD, Ito JT, Martins MDA, Tibério IDFLC, Lopes FDTQDS. Th17/Treg Imbalance in Chronic Obstructive Pulmonary Disease: Clinical and Experimental Evidence. Frontiers in Immunology. 2021; 12: 804919. https://doi.org/10.3389/fimmu.2021.804919.

[32] Nag A, Singh M, Thomas J, Ravichandran R, Gupta L, Panjiyar BK. Role of Biologic Therapies in the Rheumatic Manifestations of Inflammatory Bowel Disease: A Systematic Analysis. Cureus. 2023; 15: e45195. https://doi.org/10.7759/cureus.45195.

[33] Yu T, Yan J, Wang R, Zhang L, Hu X, Xu J, *et al*. Integrative Multiomics Profiling Unveils the Protective Function of Ulinastatin against Dextran Sulfate Sodium-Induced Colitis. Antioxidants (Basel, Switzerland). 2024; 13: 214. https://doi.org/10.3390/antiox13020214.

[34] Shao S, Chen C, Shi G, Zhou Y, Wei Y, Wu L, *et al*. JAK inhibition ameliorated experimental autoimmune encephalomyelitis by blocking GM-CSF-driven inflammatory signature of monocytes. Acta Pharmaceutica Sinica. B. 2023; 13: 4185–4201. https://doi.org/10.1016/j.apsb.2023.07.026.

[35] Gan J, Zhang H. PTPRO predicts patient prognosis and correlates with immune infiltrates in human clear cell renal cell carcinoma. Translational Cancer Research. 2020; 9: 4800–4810.

https://doi.org/10.21037/tcr-19-2808.

[36] Kato H, Perl A. Double-Edged Sword: Interleukin-2 Promotes T Regulatory Cell Differentiation but Also Expands Interleukin-13- and Interferon-γ-Producing $CD8^+$ T Cells *via* STAT6-GATA-3 Axis in Systemic Lupus Erythematosus. Frontiers in Immunology. 2021; 12: 635531. https://doi.org/10.3389/fimmu.2021.635531.

[37] Sanders JM, Jeyamogan S, Mathew JM, Leventhal JR. Foxp3+ regulatory T cell therapy for tolerance in autoimmunity and solid organ transplantation. Frontiers in Immunology. 2022; 13: 1055466. https://doi.org/10.3389/fimmu.2022.1055466.

[38] Xie F, Dong H, Zhang H. Regulatory Functions of Protein Tyrosine Phosphatase Receptor Type O in Immune Cells. Frontiers in Immunology. 2021; 12: 783370. https://doi.org/10.3389/fimmu.2021.783370.

[39] Dong H, Xie C, Jiang Y, Li K, Lin Y, Pang X, *et al*. Tumor-Derived Exosomal Protein Tyrosine Phosphatase Receptor Type O Polarizes Macrophage to Suppress Breast Tumor Cell Invasion and Migration. Frontiers in Cell and Developmental Biology. 2021; 9: 703537. https://doi.org/10.3389/fcell.2021.703537.

[40] Wang P, Ma Z, Wang Z, Wang X, Zhao G, Wang Z. MiR-6869-5p Induces M2 Polarization by Regulating PTPRO in Gestational Diabetes Mellitus. Mediators of Inflammation. 2021; 2021: 6696636. https://doi.org/10.1155/2021/6696636.